Constructional process of relatively high-relief crescent-shaped bedforms in submarine channels by gravelly sand-laden flows: analysis of the ancient case study of the Guredin palaeo-bedforms

R. Lopez Jimenez

Plaza Villafranca de los barros, 2, 2, 3; 28034, Madrid, Spain

Corresponding author email: r.lopez.jimenez00@aberdeen.ac.uk

Abstract

The channel-fills of the Miocene Alikayasi submarine channel system in the south of Turkey offer an extraordinary opportunity to improve our understanding of the physical properties of gravity-driven gravelly sand-laden flows and their resulting deposits on the seafloor. This study describes and analyses a particular area of an ancient channel-fill that is interpreted as the preserved deposits of relatively high-relief crescent-shaped bedforms consisting of conglomeratic sands (named the Guredin palaeo-bedforms). The mechanism of formation of these types of bedforms in submarine channel systems is largely speculative and normally explained by the 'cyclic step paradigm'. A comparative analysis of the Guredin palaeo-bedforms with experimental flume studies and data from modern analogues supports a new model for the construction of relatively high-relief crescent-shaped bedforms. This model proposes the formation of this type of bedform as the result a two-stage process: 1) the formation of a crescent-shaped scour by an erosional hydraulic jump (from the abrupt transition from supercritical to subcritical flow regimes), and 2) the entry of a hyperconcentrated basal flow with a basal traction carpet, which develops a separation bubble in the scour that sorts out clasts and controls their deposition (creating the final dune-like crescent-shaped morphology). This new model deals with critical questions in the design of classification systems of bedforms for gravity-driven sediment-laden flows as well as with regard the dynamics and structure of the flow events that occur in submarine channels transporting gravelly sands.

1 Introduction

Bathymetry surveys in submarine channel systems reveal relatively high-relief bedforms with variable scale and with planform morphologies similar to dunes (Wynn and Stow, 2002; Symons et al., 2016). These bedforms have been associated with gravity-driven sediment-laden flows and explained through hypotheses that have continuously evolved, as the understanding of their physical properties and quality of data from real-wold cases has improved (e.g. Bouma and Treadwell, 1975; Piper and Savoye, 1993; Wynn et al., 2002; Fildani et al., 2006; Smith et al., 2007; Hughes Clarke, 2016). The cyclic step paradigm is commonly used to explain the formation of trains of bedforms that show crescent-shaped morphologies in planform view (Normark and Piper, 1991; Fildani et al., 2006; Lamb et al., 2008; Normandeau et al., 2014; Tubau, 2015; Zhong et al., 2015; Hughes Clarke, 2016). The flow dynamics and sedimentary basics of this paradigm are the following: 1) a repetitive sequence consisting of a supercritical flow on the lee-side of a step, an erosional hydraulic jump at its bottom (implying the formation of a scour) and followed by a subcritical flow, usually over an upstream dipping slope (Parker and Izumi, 2000; Kostic et al., 2010); 2) the upstream migration of the hydraulic jumps, and thus the scour, during flow events (e.g. Cartigny et al., 2011; Kostic, 2011); and 3) cyclic steps involving deposition show an internal sedimentary architecture consisting of a series of upstream-dipping bed sets (i.e. backsets) bounded by comparatively steep downstream-dipping truncations (e.g. Fildani et al., 2006: Cartigny et al., 2011). Sediment-laden flows transporting relatively fine-grained sediments (mud to sand) are normally associated with the cyclic-step paradigm (Normark et al., 1980; Migeon et al., 2001; Fildani et al., 2006; Hughes Clarke, 2016).

There are a comparatively small number of studies that have shown solid evidence of relatively high-relief bedforms consisting of gravelly sands in the thalwegs of submarine channel systems (e.g. the Laurentian Fan, Piper et al., 1985; the Var canyon, Malinverno et al., 1988; the Hikkurangi channel system, Lewis and Pantin, 2002; the Monterey canyon, Paull et al., 2010, 2011; the Setúbal Canyon, Arzola et al., 2008). The cyclic step paradigm has also been suggested to be valid for the formation of high-relief bedforms by gravelly sand-laden flows (Postma et al., 2014; Symons et al., 2016). However, data and observations from the Monterey Canyon challenge the application of the cyclic step paradigm to the origin of its high-relief bedforms consisting of gravelly sands (see discussion in Paull et al., 2010). The sedimentary architecture of the deposits beneath gravelly sand bedforms is so far assumed to be

massive, with a poorly graded and sorted structure, without internal stratification (Shor et al., 1990; Paull et al., 2010). These assumptions need further evidence from real-world data sets, whose collection is handicapped by different issues, for example: a) direct observations or measurements of the properties of gravelly sand-laden flows in modern environments are extremely difficult because of their destructive character and from technological limitations on their measurement (Paull et al., 2010; Sumner and Paull, 2014); b) no internal structure can be inferred from seismic sections beneath gravelly sand bedforms, probably because of their low impedance contrast (e.g. Paull et al., 2010, 2011); c) the reproduction of flows containing large clasts in the laboratory are difficult to achieve and parameter scaling is also problematic (e.g. Postma et al., 1988); and d) ancient outcrop case studies of bedforms consisting of conglomeratic sandstones are particularly scarce and consist of structures of smaller scale than those surveyed in modern cases (e.g. Winn and Dott, 1977; Piper and Kontopoulos, 1994; Ito and Saito., 2006).

As the origin of high-relief bedforms is still poorly understood, it is necessary to provide more evidence on the physical mechanisms related to their formation as well as a general understanding of the physical properties of their parent flows. The study of exceptional ancient deposits of submarine channel-fills, analogues to certain modern case studies, can show data of great value for the research on this topic (with unmatched detail). The present work shows the sedimentary architecture of interpreted relatively high-relief crescent- shaped bedforms consisting of conglomeratic sands from an exceptionally well exposed case study on an ancient channel-fill.

2 Data collection on the outcrop: the sedimentary architecture analysis

The analysis of the outcrop of this case study is largely based on the original approach of Allen (1983) and Miall (1985). It differentiates two major groups of features in sedimentary deposits: bounding surfaces and sedimentary facies. Bounding surfaces are most of times lineal features that can be observed on the outcrop (normally as the intersection of surfaces on two-dimensional exposures). They are noticeable to naked eye observations because of changes in both the geometrical relationships of strata/beds (i.e. unconformities or truncations) and the physical properties of the sediment, which makes the ‘sedimentary facies’ (e.g. clast-size, clast-orientation or lithology). Bounding surfaces can be observed at a wide range of scales, geometries and cross-cutting relationships among each other. Their

differentiation allows the determination of the sequence of formation or hierarchy of sedimentary deposits (Friend et al., 1979; Allen, 1983; Mutti and Normark, 1987).

The description of exposures will use the following terminology for establishing their orientations with respect to the average palaeocurrent direction: ‘strike cross-section’ will refer to exposures that are oriented approximately perpendicular to the average palaeocurrent direction, whereas ‘downslope section’ will do so for those approximately parallel to the palaeocurrent direction.

There is variable understanding and use of certain basic terms for the description of sedimentary deposits in the literature. In order to avoid misunderstandings, the basic terminology used in the present study is defined as follows: 1) ‘Bedform’ is used to describe the bathymetrical aspect of the sediment on the seafloor at a given time; when dealing with reconstructed bedforms from ancient deposits, the palaeo- prefix is added. The term ‘scour’ will strictly be used as a bathymetrical feature as part of a bedform with a relative elongated low-relief caused by the erosion of a flow. Palaeo-scour will be used for those bounding surfaces whose attributes that can be interpreted as a ‘healed’ ancient scour on the sedimentary record (typically truncations truncate a series of beds that show a concave-up morphology when they are exposed through oblique or strike cross-sections). The deposit overlying or filling the palaeo-scour is also referred as scour-fill (compare with definition of scour in Mutti and Normark, 1987); 2) ‘Bed configuration’ is used for the description of the geometrical attributes of a series of bounding surfaces on particular areas of the deposit constrained by other key bounding surfaces (e.g. low-angle cross-bedding constrained); it is also used to define cross-cutting relationships among these areas (e.g. onlap, downlap); 3) ‘Sedimentary facies’ includes the description of any sediment attribute (e.g. distribution of values of size, orientation, roundness and lithology of clasts). 4) ‘Sedimentary architecture’ is the integration of bed configuration and sedimentary facies.

The description of the sedimentary architecture of the Guredin palaeo-bedforms is preceded by a more general one of the canyon-fill where they crop out. The discussion section starts with the analysis of the sedimentary architecture of the Guredin palaeo-bedforms and its interpretation. This is followed by comparative analysis with experimental and real-wold case studies for the discussion of the particularities of constructional processes of deposits by gravelly sand-laden flows.

3 The Alikayasi submarine channel system

The Guredin palaeo-bedforms (subject of this study) are constituent deposits of the ancient Alikayasi submarine channel system (Lopez Jimenez, 2017; 2018). This system developed in the Miocene Maras Basin, located in the south of Turkey (Figure 1). The Maras Basin also contains other deepwater sedimentary systems (Cronin et al., 2008; Gul et al., 2011, 2012; Lopez Jimenez, 2017). The channel systems that developed in the Maras Basin incised into mud-silt sediments (i.e. hemipelagites) that aggraded during the Serravallian Age (Miocene). Two fold-and-thrust belts propagated in almost perpendicular directions during the evolution of the Maras Basin. The northern fold-and-thrust belt corresponds to the present-day Engizek Fault Zone (which integrates into the Bitlis-Zagros Suture Zone, see Figure 1) and propagated approximately from north to south. The western fold-and-thrust belt starts from the east at the Misis-Andirin mountain range which shows a west to east propagation progressively veering towards a north-west to south-east direction (linking this belt with the East Anatolian Fault Zone, see Figure 1). The latter belt controlled the evolution of the Alikayasi system by the development of localised subsidence between two major propagating thrusts, promoting a major sediment pathway with a north-east to south-west direction for tens of kilometres. This fold-and-thrust system is thought to have reached the hinterland, enabling a continuous sourcing of gravelly sands with a wide-range of lithologies to the deep-sea, with the probable development of fan systems in the proto-Iskenderun Gulf during the Miocene (Lopez Jimenez, 2017).

The Alikayasi system consists of four major channel-fills that have been categorised as (palaeo)canyons because to the maximum dimensions they could have developed (the largest ~5 km wide and ~550 m deep and the smallest ~700 m wide and ~150 m deep). This system ends with tens of vertically stacked minor channel-fills that pile up for ~3 km. The stacking pattern of the channel-fills of this system shows a lateral offset to the SE, which is interpreted to have been controlled by the propagation of the aforementioned two major thrusts of the western fold-and-thrust belt (Lopez Jimenez, 2017). Biostratigraphical analyses have suggested palaeo-depths of the system ranging from 350 to 750 metres at areas that correspond to the last (i.e. youngest) channel-fills of the Alikayasi system that crop out to the SW (Hüsing et al., 2009).

4 The CS3 canyon-fill

The Guredin palaeo-bedforms are part of the second canyon-fill of the Alikayasi system (the CS3 Canyon-fill). This canyon incised into the uppermost part of the first canyon-fill, cutting intracanyon channel-fills dominated by conglomeratic sandstones, debrite type deposits and mudstone (Lopez Jimenez, 2017). The excellence of the outcrops of these palaeo-bedforms resides in the unusual quality and diverse orientation of the exposures but also in the reliable interpretation of its large-scale setting (the CS3 Canyon-fill). The palaeocurrent measured on this canyon-fill (from flutes) show a consistent ENE to WSW palaeo-flow direction (Figure 2), which is slightly different from the rest of the canyons (i.e. NE to SW). Conversely, clast imbrication proved highly inconsistent when measured on different areas of the same canyon-fill. The slope gradient at the Guredin palaeo-bedforms could not be determined, as usual in ancient outcrop case studies.

The CS3 canyon-fill consists of three major filling phases defined by second order concave-up bounding surfaces (Figure 3). They connect each other at their axes and are vertically stacked with a lateral offset to the south-east. The Alikayasi Thrust, as part of the western fold-and-thrust belt, is thought to have caused this offset as the axis of the CS3 Canyon was displaced to the south-east by the propagation of the Alikayasi thrust concomitantly to the filling of the CS3 canyon (Lopez Jimenez, 2017). The edge of the north-western margin of the CS3 canyon-fill has been eroded because of the pervasive fracturing related to the propagation of the Alikayasi Thrust. This eroded NW margin has been included in a sketch that reconstructs the approximate architectural framework of the CS3 canyon-fill (Figure 3).

Biostratigraphical data from Önalan (1986) and Lopez Jimenez (2017) has provided evidence of the marine character of the CS3 canyon-fill deposits (e.g. foraminifera, coral and algae fragments). The three filling phases of the canyon-fill are dominated by a bed configuration of amalgamated low-angle cross beds (<5°) with an average maximum clast-size is in the pebble range. These amalgamated conglomeratic sandstones show both inverse and normal grading (the former especially at the first canyon filling phase). The texture description and analysis of the maximum clast size of the canyon-fill facies points to the interpretation of a deposition by traction-carpet basal flows (Lopez Jimenez, 2017). On the other hand, sequences with high-angle foresets crop out to the top NNW margin and off-axis areas of the third filling phase (see Figure 3). These sequences consist of conglomeratic sandstones

with an average maximum clast size in the cobbles range (but also with occasional boulders). The analysis of the exposures of these outcrops with comparatively large clast size deposits reveal dune-like geometries with foreset bed configurations (see Lopez Jimenez, 2017). This study focuses on one of the best exposed of these sequences (the Guredin palaeo-bedforms) which is located to top of the Guredinkalesi hill (Figure 4). Other outcrops with similar characteristics crop out further to the south-west (see yellow star in Figure 2 and Figure 3). Both the Guredin palaeo-bedforms and the other outcrops are thought to be part of a series of bedforms that developed during a similar and relatively narrow time span along the canyon-floor. This is based on the palaeocurrent data obtained for the CS3 canyon-fill (i.e. ENE to WSW): the Guredin palaeo-bedforms and the other outcrops with the interpreted dune-like bedforms are contained in a virtual line that follows the CS3 canyon-fill palaeocurrent direction (ENE to WSW direction with an angle of dip of 15°). See the alignment of the two areas with these types of palaeo-bedforms in Figure 2.

5 The sedimentary architecture of the Guredin palaeo-bedforms

5.1 General view of the outcrop

The Guredin palaeo-bedforms crop out near the top of the Guredinkalesi hill (at viewpoint P1 in Figure 2). Two major vertical sections, approximately orthogonal one to another, expose the sedimentary architecture of the Guredin palaeo-bedforms (see lines 1 and 2 in Figure 4). A third vertical section, smaller but relevant for the interpretation of these deposits, completes the main exposures that have been analysed (see line 3 in Figure 4). The term ‘section’ will always be used when referring to the vertical exposures related to any of the lines indicated in Figure 4. This figure and subsequent ones show six white circles labelled A to F. These are spatial reference points meant to facilitate the location of different parts of the outcrop in following figures (and provide reference for a three-dimensional reconstruction). The exposures located to the easternmost part of the Guredinkalesi hill (nearby points ‘C’ and ‘B’) are described in less detail because of their difficult access. Image rendering issues when using a long-focus lens to take photographs (i.e. chromatic aberration) makes unreliable facies descriptions in the scale of decimetres or less only from the obtained images (e.g. Figure 7). For this reason, facies attributes remain uncertain on the areas where it was not possible to observe in this scale range (even with binoculars).

The view of Guredinkalesi hill from viewpoint P2 shows the Guredin palaeo-bedforms along a line generally slightly oblique to the ENE to WSW palaeocurrent flow direction in the ancient CS3 canyon (Figure 5). This view allows the observation of the aforementioned three vertical sections or main exposures (lines labelled 1 to 3 in Figure 4). The general view of the Guredin palaeo-bedforms shows how the dominating low-angle cross-beds consisting of amalgamated pebble sandstones in the CS3 canyon-fill is broken by a series of deposits constrained by unconformities or truncations (thickest black line tracing in Figure 5). These deposits show areas with comparatively large clast-sizes and beds with high angle of dip. They have been grouped into three sequences according to the truncations and organised in a younging direction. Sequence 1, 2 and 3 are always drawn in subsequent figures in colours blue, yellow and green respectively.

5.2 Description of sequences

5.2.1 Sequence 1

Figure 5 shows this sequence through exposures with different orientations (right-angled marks labelled 90˚ indicate vertices of two roughly orthogonal exposures in Figure 5). The lower bounding surface of Sequence 1 shows both straight and irregular morphologies (see the bottom boundary line of the blue area in Figure 5). Starting from the east (point ‘B’), the strike cross-section of this lower bounding surface is irregular and has an average angle of dip of ~40-50°. This part truncates underlying low-angle cross-beds of pebbly sandstone following the palaeo-canyon downslope direction from ENE to WSW, inferred from the measured average palaeocurrent direction. The deepest point of the truncation lies ~100 m further to the west after having ‘incised’ into a vertical section of ~20 m of low-angle cross-bedded pebble sandstone (see point ‘A’). The exposure corresponding to line 3 in Figure 4 shows how the degree of incision of this truncation also varies in a strike direction (Figure 6). The truncation loses its cross-cutting character further downslope (i.e. to the west) becoming conformable with respect to the predominant pebbly sandstones (from point ‘A’ towards point ‘D’ in Figure 5). The strike and dip where these pebbly sandstones lie on the upper bounding surface of Sequence 1 is 080˚/5˚N (measured next to point ‘D’).

The bed configuration of the deposits of Sequence 1 through a downslope section consists of foresets that terminate as a downlap over the irregular truncation of its lower bounding surface (Figure 5). These foresets are product of amalgamated beds of variable clast-size, alternating clast-supported cobbly and

pebbly sandstones. Through a strike cross-section (line 3 of Figure 4), these foresets are so clear due to the lichen that has grown over the exposure. Notwithstanding, it can be observed clast-supported pebbly sandstones at the bottom of Sequence 1 abruptly change to clast-supported cobbly sandstone (Figure 6). This abrupt change coincides with the bounding surface of a foreset that can be observed from the distance with binoculars (traced in Figure 5). The strike cross-section of Sequence 1 shows a rapid fining upward on its top part (1-2 m thick) in the form of amalgamated sandstone beds. The top of the last sandstone bed defines here the upper bounding surface of Sequence 1, which has an angle of dip ~10˚ to the west.

Some areas of the Sequence 1 show 'holes' with shapes of contorted ellipsoids and others with more angular shapes ranging from a few centimetres to more than a metre in diameter (see Figure 6). Some of these holes are coated with fine-grained sediment (apparently silt-to-sand size). These can be interpreted as remnants of rip-ups of unknown deposits that have eventually fallen off the exposure.

5.2.2 Sequence 2

Most of Sequence 2 crops out mainly through a downslope section and, separated, a comparatively small one shows both downslope and strike cross-sections (see the smaller one above point 'D' in Figure 5 and the small area encircled in dashed white line in Figure 7). These exposures are separated by a ~7 m long exposure corresponding to the lowermost part Sequence 3 (see the area between the two black arrows in Figure 7). Figure 6 shows the straight geometry of the bounding surface between sequences 1 and 2. This exposure shows deposits of Sequence 2 as boulder-sized blocks; the smaller in a position that suggests a recent gravitational displacement (so not reliable for this analysis) while the largest one seems to be *in situ*. Sequence 2 is part of the predominant low-angle cross-bedded amalgamated pebbly sandstone of the CS3 canyon-fill at its easternmost part (see areas to the east of points 'C' and 'D' in Figure 5). The lowermost part of Sequence 2 at its western edge shows a progressive increase in the angle of dip of bedding. This change in the bed configuration occurs exactly over the concave-up morphology of the upper bounding surface of Sequence 1. These beds show a relatively gentle downlap termination over the deposits of Sequence 1. The downlap is also observed in the aforementioned smaller deposit located further to the west (Figure 7 and Figure 8).

Figure 8 shows a close-up of the smaller exposure of Sequence 2, which is oriented slightly oblique to the ENE-WSW palaeocurrent direction (see its location in Figure 7 at the white dashed-lined rhombus

tagged S2-1). The bottom of this figure shows a line tracing of the observed clasts whose longest axes are at least 1 cm long. The not drawn clasts are a variable mixture that covers from small pebbly sandstone to coarse-sand (small pebbles and granules appear frequently clast-supported). The facies is dominated by amalgamated deposits of matrix-supported pebbly sandstone, with areas of clast-supported cobbles and large pebbles (the latter responsible of the downlap that can be discern from afar). These areas of cobbles and large pebbles show a variable concentration. The clast orientations do not suggest a clear imbrication pattern. The distribution of clast sizes reveals the surface of amalgamated deposits with a dip direction to the NNW. This means that the bed configuration of Sequence 2 in this area is not only defined by a downlap to the west over the deposits of Sequence 2 but also towards an oblique or even perpendicular direction (~NNW) rendering a mound-like geometry in 3D.

5.2.3 Sequence 3

The sedimentary architecture of Sequence 3 is exposed through roughly two orthogonal sections (see lines 1 and 2 in Figure 4). The upper bounding surface of Sequence 3 in this section shows a concave upward curvature (see the white arrows pointing perpendicularly to this surface in Figure 7). The predominant low-angle cross-bedded pebbly sandstones overlying the NNW of Sequence 3 meet its upper bounding surface by up-dip terminations (see the onlap of these deposits over the upper bounding surface of Sequence 3 marked with white arrows in Figure 7). It is important to emphasise that this surface in is shown thorough an oblique view in Figure 7, and the exposure containing it is perpendicular to the palaeocurrent direction (see Figure 4 for spatial reference). The lower and upper bounding surfaces of Sequence 3 on this strike cross-section describe a triangular geometry (see Figure 5 and Figure 7). The deposits constrained by these surfaces show a bed configuration defined by a concave-up bedding pattern that is truncated by the upper bounding surface of Sequence 3 (see thin black lines inside the area defined by points ‘D’, ‘E’ and ‘F’ in the photo-interpretation of Figure 5 and the dashed black line tagged ‘bedding’ in Figure 7). On the other hand, the exposure of Sequence 3 through a downslope section shows its irregular lower bounding surface dipping ~30˚ to the west and truncating deposits of Sequence 2 (see surface from point ‘C’ to ‘D’ in Figure 5). Its upper bounding surface dips ~5˚ to the west and it is overlain by the predominant low-angle cross-beds of the CS3 canyon-fill as an onlap termination.

A large part of the exposure of the strike-cross section of Sequence 3 is accessible for data collection directly over the exposure. Seven logs were measured at the bottom part of this section (see the location of each log over the exposure indicated by lines of different colours in Figure 7). The total length of each log is 2 m, corrected from longer measured sections to a true dip direction (taking as reference bedding planes observed on the concave upward upper bounding surface of Sequence 3). These logs show measurements of the longest axes of the largest clasts observed every 10 cm over the younging direction, and searching across a 1 m wide strip of outcrop (Figure 7). The maximum measurement was of 10.5 cm (although it is greater than the measurement spacing of 10 cm, these clasts were exceptional, and thus could be fitted into one interval). The average (i.e. arithmetic mean) and mean deviation values for the measurements of each log are indicated beneath each line graph (see label AVG and MD respectively, at the bottom of Figure 7). The mean deviation was chosen instead of the standard deviation to express a more efficient dispersion of data from the average value (since it is not the intention to estimate the dispersion from a perfect Gaussian data population; see Gorard, 2005). The average values of the clast-size show a tendency to decrease from the thickest to the thinnest part of the strike cross-section of Sequence 3 (i.e. from log 1 to log 7). This is even more remarkable considering the predominant cobble size and occasional boulders observed (not possible to log without climbing equipment) on the thickest part of Sequence 3 (see Figure 9). This tendency of clast-size decrease is not perfectly continuous, as two of the average clast-size values indicate. Logs 2 and 6 break what would be a perfect clast-size decreasing tendency by the occurrence of areas of comparatively large clasts (i.e. cobbles) over the exposure (usually clast-supported). Most of the time these areas are small and well constrained (see example on the centre of the top photo in Figure 10). However, there are at least two areas with clast-supported cobbles that stretch for several tens of metres from the thickest part of Sequence 3 towards its tip (from line ‘E’-‘D’ to point ‘F’ in Figure 7). These ‘cobble stripes’ are part of the sedimentary features that render the concave-up morphology of the bed configuration from afar (see the dashed black line of Sequence 3 in Figure 7). The relatively high values of mean deviation in each log derive from these areas of relatively large clasts (see MD values in Figure 7). The clast-size population becomes smaller to the upper part of Sequence 3 at any reach of the strike cross-section. The facies immediately beneath the upper bounding surface of CS3 consists of isolated and occasional small pebbles in predominant coarse-grained sandstone.

5.2.3.1 PERVASIVE IMBRICATION

An area with pervasive imbrication is here defined as that where more than 50% of the clasts from medium pebble to cobble size classes show exactly the same values of angle of dip and direction measured on the plane defined by the a-b clast axes (i.e. the longest ones perpendicular one to another). The pervasive imbrication is particularly noticeable because of the abundant oblate clasts, which show an overlapping arrangement of their relatively flat surfaces.

The deposit constrained by the upper and lower bounding surfaces of Sequence 3 shows, at its westernmost part, a lineation pattern from afar dipping ~50˚ to the WSW (see the parallel black thin lines in Figure 5). In a closer range this lineation reveals itself as a pervasive imbrication of cobbles and boulders (Figure 7). This pervasive imbrication is also observed in cobbles and pebbles of the thickest part of the strike-section of Sequence 3 (i.e. from log 1 to 4 in Figure 7). The imbrication dip direction veers from 150˚ to 100˚ along a north to south direction over the strike-section of Sequence 3 (see imbrication data embedded in line graphs of Figure 7 and in Figure 9). The most clearly exposed imbrication patterns crop out on the westernmost part of the downslope section of Sequence 3 (Figure 9).

The dip direction of the imbrication veers rapidly (i.e. in 2-3 m) next the corner of the lower part of the deposits of Sequence 3 (see curved black arrows on the left of the top photo in Figure 9). This veering coincides with an also rapid transition from areas dominated by clast-supported cobbly-pebbly sandstone to clast-supported cobbly sandstone with occasional boulders. The azimuth of imbricated clasts changes more gradually from the middle part to the corner of the strike cross-section of Sequence 3. One of the largest areas of pervasive imbrication lies above Log 2 (Figure 10), with values very similar to other measured on the strike cross-section (Dip direction=305˚ and Angle of dip=40˚). The imbrication is not noticeable at the uppermost part of Sequence 3 in both downslope and strike cross sections as well as on its easternmost part (the latter close to point ‘C’ in Figure 5). The clast-size in this part appears to be finer compared to that where the pervasive imbrication since no boulder-size clasts could be observed from long-focus photography (but apparently consisting of clast-supported cobbly-pebble sandstones).

6 Discussion

This section aims the reconstruction of the 3D morphology of the Guredin palaeo-bedforms and the interpretation of the hydrodynamics of the sediment-laden flows that produced them. This interpretation is supported by a comparatively analysis of the sedimentary architecture of the Guredin palaeo-bedforms with data from both experimental modelling and data sets from relatively high-relief bedforms in modern submarine channels consisting of gravelly sands.

6.1 Major erosional features as crescent-shaped scours originated by hydraulic jumps

A relatively large-scale analysis of the sequences of the Guredin palaeo-bedforms results in the differentiation of major erosional and depositional features. The major erosional features correspond to the lower bounding surfaces of sequences 1 and 3, which truncate underlying pebbly sandstones with relatively low-angle cross-bed sets. The depositional features correspond to the bulk sedimentary deposit of each of the three differentiated sequences, consisting of amalgamated conglomeratic sandstone deposits with variable bed configurations and average clast-size spatial distribution (Figure 5).

The irregular lower bounding surfaces of sequences 1 and 3 are here interpreted as crescent-shaped scours developed by hydraulic jumps because of a series of morphological attributes that are discussed below. The morphology of these bounding surfaces through a downslope section is similar to that of crescent-shaped scours surveyed in modern submarine channels and other marine settings (e.g. Wynn et al., 2000; Fildani et al., 2006; Paull et al., 2011; Tubau et al., 2015; Zhong et al., 2015; Hughes Clarke, 2016). Downslope sections of these real-world examples typically show a chute-and-pool morphology (particularly when crossing the inflexion point of the crescentic planform morphology). The ‘chute’ is a two-dimensional feature with a concave morphology that results from a downslope dipping section through the step or lee-side of three-dimensional crescent-shaped scour. Similarly, the ‘pool’ corresponds to a relative bathymetry low located along the bottom of the main step. The chute-and-pool term is here used strictly as bathymetrical morphology without considering any aspect of the constructional process (compare with Taki and Parker, 2005 and Cartigny et al., 2014).

The lower bounding surfaces of Sequences 1 and 3 show the aforementioned chute morphology through the downslope section (Figure 5). The exposure that shows a strike cross-section of the lower

366 bounding surface of Sequence 1 is located at the lowest part of the chute and shows a pronounced
367 concave-up morphology that cuts underlying bed sets (Figure 6). This morphology is compatible with
368 the existence of relative bathymetry lows (i.e. pool) observed in some real-world case studies that are
369 normally located at the bottom of the main step and by the inflexion point of its crescentic planform
370 morphology (see bathymetric contours of bedforms in Paull et al., 2010 and Zhong et al., 2015). In the
371 case of Sequence 3, its lower bounding surface only shows an incision or palaeo-scour at the end of the
372 chute morphology (see the lowermost part of Sequence 3, constrained by two black arrows that point to
373 two separated deposits of Sequence 2 in Figure 7). It is possible that the direction of the exposure of
374 this bounding surface is laterally offset with respect to a perfectly central downslope section of a palaeo-
375 crescent-shaped scour (i.e. cutting though the inflexion point of the crescentic morphology of the step).
376 Indeed, the most noticeable 'pool' morphology would be obtained if the downslope section cuts the
377 central part of the scour (where the aforementioned relative bathymetry lows could lie). Another
378 possibility is that the crescent-shaped scour did not develop such relative bathymetry low, but just a
379 chute-like morphology with a subtle upstream-dipping slope after the chute. Scours with this type of
380 morphology have been obtained in steps reproduced in the laboratory (e.g. Taki and Parker, 2005;
381 Cartigny et al., 2014) and from bathymetric surveys in submarine channels (e.g. Mitchel, 2006; Paull et
382 al., 2011).

383 There is an additional feature that supports the interpretation of a crescent-shaped scour in the case of
384 the lower bounding surface of Sequence 3. The deposits that onlap this surface (Figure 7) terminate to
385 the north in a wall or cliff that describes an arcuate morphology (see the arcuate lineation in Figure 4).
386 This arcuate lineation matches a line tracing of what would be the planform view of the northern half of a
387 crescent-shaped step (starting from point 'C' to 'F'). Differential erosion can explain this arcuate
388 lineation (actually a surface in the field). The predominant pebbly sandstones deposited around the
389 northern edge of those that comprise Sequence 3 appear to have been easily removed by weathering
390 (exposing the 'fossilised' geometry of the interpreted crescent-scour).

391 The formation of crescent-shaped scours has been associated with the development of an erosional
392 hydraulic jump (e.g. Mutti and Normark, 1987; Kostic and Parker, 2006; Postma et al., 2009). The
393 formation of these morphologies in submarine canyons filled with gravelly sands has also been
394 proposed as result of retrogressive breaching failures or local slope instability caused by thrusting (Paull

et al., 2011 and Duarte et al., 2010 respectively). The irregular path of the lower bounding surfaces of Sequence 1 and 3 supports an erosional process caused by a hydraulic jump. These irregular surfaces (i.e. a series of high and lows) are better explained by the ripping-up of sediment of the CS3 canyon floor by the effect of “extreme minimum pressures” that caused uplift pressures (Chanson, 2004). The observed rip-ups in Sequence 1 could be seen as evidence of this process, but they could have also been transported from other areas situated farther upslope. The inference of a hydraulic jump implies that the flow event responsible for the palaeo-scours previous of the deposition of Sequence 1 and 3, evolved from a supercritical regime to a subcritical one at this particular area of the CS3 canyon (i.e. by the north-western canyon-wall; see Figure 2). Considering the low-angle cross bed configuration of the predominant facies of the CS3 canyon-fill, the hydraulic jump that formed the first palaeo-scour (associated with the lower bounding surface of Sequence 1), developed on a canyon-floor with bedforms whose amplitude would have been in the order of decimetres (see stage 2 of Figure 11 with parallel bedding for simplification). In the case of the second palaeo-scour (associated with the lower bounding surface of Sequence 3), it can be observed a subtle relief on the upper bounding surface of Sequence 2 through a downslope section (Figure 5). This relief can be interpreted as a gentle step that could have promoted the second hydraulic jump that is interpreted for the lower bounding surface of Sequence 3 (see stage 4 and 5 of Figure 11). This hydraulic jump promotion would have occurred following the same morphological control to flow regimes described for cyclic steps (Kostic et al., 2010).

Following the cyclic step paradigm, the chute (or step in 3D) created by the erosive hydraulic jump would have promoted a relatively small section of the flow in a ‘more supercritical’ state than that immediately upstream (i.e. defined by a comparatively shallow and fast flow). This situation would have caused the upstream migration of the hydraulic jump by the erosion of the substrate on the chute, leading to the formation of the classic backset bed configuration. In the case of the Guredin palaeo-bedforms an upstream migration of a hydraulic jump accompanied of deposition is ruled out because of the foreset bed configuration of the scour-fill deposit and absence of backsets in any of the described sequences. Had the sediment ripped up by the hydraulic jump been deposited into the scour, the scour-fill would show either a backset bed configuration (typical of ‘net-depositional cyclic steps’; see Fildani et al., 2006) or an unstructured deposit (similar to that described by Postma et al., 2009).

6.2 The crescent-shaped scour as the base for a constructional model

The interpretation of crescent-shaped scours as product of hydraulic jumps is the base for a hydrodynamic model that enables the reconstruction of the 3D morphology of Sequences 1 and 3 as scour-filling deposits with a dune-like morphology (focused on the analysis of Sequence 3 because of a comparatively large amount of data available).

The incision observed in the strike cross-section of Sequence 1 (Point 'A' in Figure 5 and Figure 6) is here interpreted as analogue to the relative bathymetry lows usually observed at the bottom of crescent-shaped steps. The position of these lows roughly at the inflexion point of the crescentic shape of the step agrees with a theoretical similar point for the arcuate lineation shown in Figure 4 (which has been interpreted as the planform relic of the crescent-shaped scour where Sequence 3 deposited). A virtual line parallel to the palaeocurrent direction crossing point 'A' in Figure 4 would divide two roughly mirror images of a perfectly symmetric crescent-shaped scour (i.e. a line of symmetry). The assumption of a perfect crescentic shape facilitates the extrapolation of the rest of the deposit of Sequence 3, assuming also similar hydrodynamic mechanisms in both mirror sides of the crescent-shaped scour.

6.3 A dune-like deposit filling a crescent-shaped scour

Following the symmetry principle, the complete sedimentary architecture of Sequence 3 has been reconstructed in Figure 12. The creation of a mirror image of the half-lens geometry of Sequence 3, flipped to the SSE, results in a dune-like morphology with a downslope crest dipping ~5˚ to the WSW (following the palaeocurrent direction measured in flutes of the CS3 canyon-fill). The very central part of this dune-like deposit (i.e. the crest) has been eroded, since the upper bounding surface of Sequence 3 in the field does not show the expected concave-down curvature (see the upper bounding surface of Sequence 3 at the crest in the upper left sketch in Figure 12). The grain size distribution and imbrication data of Sequence 3 has been summarised on the two sketches to the left of Figure 12. Following the symmetry principle, the cobbles and occasional boulders observed at the corner of Sequence 3 are thought to have dominated the very core of Sequence 3 (eroded). The clast-size data from logs and general observations on the exposures can be synthesised in three main clast-size zones with the following predominant facies: clast-supported cobbly sandstone with occasional boulders, clasts-supported cobbly-pebbly sandstone and matrix-supported pebbly sandstone. The spatial distribution of

these zones shows a decrease in size and proportion of the largest clasts from the axis to the margins of the dune-like deposit. At least two major 'cobbly stripes' stretching into the matrix-supported pebble sandstone zone (observed in the strike cross-section of Sequence 3) are depicted in the strike-cross section of the 3D reconstruction (see medium grey appendices that follow bedding in the top sketch of Figure 12). The downslope section sketch (top right of Figure 12) shows the internal clast-size distribution near the axis of the dune-like deposit (see red line for reference). This distribution is not as accurate as that from the strike cross-section because of the inaccessibility to the exposure on the easternmost part of the section (which prevented logging of clast size measurements). The question mark on sketch of the downslope section denotes the uncertainty on the predominant clast-size of that area. Notwithstanding, examination with a long-focus lens has allowed the identification of clast-supported cobbly-pebble sandstones but no boulders (through visual comparison of clasts sizes between inaccessible and accessed exposures).

The dip directions measured on imbricated clasts have been plotted over the reconstructed complete strike cross-section of the dune-like deposit (see arrows with white-filled heads in the sketch at the bottom of Figure 12). The pattern of these arrows represents the observed change from 330˚ to 280˚ in the dip direction of imbricated clast from the off-axis to the axial parts of Sequence 3 (see Figure 7). This veering has also been extrapolated in the mirror image of the dune-like geometry to the SSE.

6.4 Palaeocurrent interpretation from clast imbrication

What is the palaeocurrent direction that can be inferred from the imbrication data associated with the deposition of Sequence 3 into a scour with a possible crescentic shape? The observed pervasive imbrication in Sequence 3 dips to a direction ranging from W to NNW (i.e. 280˚ to 330˚). These dip directions are in a range similar to the ENE to WNW direction inferred for the canyon-fill where the Guredin palaeo-bedforms were formed (i.e. the CS3 canyon-fill) as well the predominant palaeo-current direction of the Alikayasi system (Lopez Jimenez, 2017). This situation would categorise the observed imbrication as 'reversely-oriented' since a palaeocurrent direction is expected to be opposite of the dip direction of imbricated clasts (Galvin, 2003). Reversely-oriented imbrication has been interpreted as product of three major processes: 1) scouring of sand beneath the downslope side of the clasts; 2) sliding of clasts over relatively steep slopes of the lee-sides of dunes or ripples; and 3) pivoting about thick end of clasts with wedge or pear shapes (Galvin, 2003). There are a series of observations that

contradict any of these three explanations for the interpretation of a reversely-oriented imbrication. The 'scouring' explanation is associated with the presence of sand beneath the reversely imbricated clasts (i.e. matrix-supported) in foreset be configurations. The pervasive imbrication of Sequence 3 has been found in clast-supported ungraded fabrics where no foresets are discernible. The 'sliding' explanation is also associated with the presence of fine grained sediment (mud or sand) over slopes of dunes where larger clasts (pebble to boulders) with oblate shapes can slide. Again, the predominant clast-supported fabric of the areas with pervasive imbrication does not fit the expected sedimentary architecture of a deposit where sliding occurred (i.e. isolated matrix-supported clasts with their flat surfaces oriented in the same direction as foresets). The 'pivoting' explanation is associated with 'sheet flows', a type of flow that does not fit with the filling of a scour but with deposition over a relatively flat surface.

It is not possible from this study to discard absolutely any of these explanations or other possible ones in order to interpret reversely-oriented clasts in the observed imbrication of Sequence 3. However, there is an alternatively explanation for the measured imbrication assuming the occurrence of backflows over the lee-side of the forming dune-like deposit of Sequence 3 (i.e. opposite to the ENE-WSW palaeocurrent direction of the CS3 canyon-fill). This interpretation would categorise the imbrication as 'regularly-oriented' (Galvin, 2003). The interpretation of backflows from the regularly-oriented imbrication on the lee-side of the dune-like deposit of Sequence 3, its clast-size zonation and the foresets observed in Sequence 1 are observations that have led to the hypothesis of a flow separation as the mechanism responsible for the deposition of these sequences. This type of hydrodynamic mechanism has been described and analysed in detail by Allen (1968, 1982) focused on the understanding of the hydrodynamics of flows associated with the construction of ripples and dunes. The following section uses the results of Allen's experiments with flow separation in steps for proposing a model that explains the construction of Sequence 3 (and possibly Sequence 1), which could also be applied for certain crescent-shaped bedforms found in modern submarine channels analogue to CS3 canyon-fill (i.e. filled with gravelly sands).

6.5 Comparative analysis with experimental modelling: flow separation as a mechanism for the construction of a dune-like bedform in a crescent-shaped scour.

Allen (1968) run flume experiments with subcritical flows in steps of different geometrical configuration to test theoretical modelling focused on the formation of ripples. He set plaster models of 'reverse

closure negative steps' that are analogues of submarine crescent-shaped scours (see chapter 10 of Allen, 1968). Flows had a mean velocity between 35 and 55 cm/sec, always in the subcritical regime and moderately turbulent (Reynolds number ~10^4). The geometry of the flute marks on the plaster surface of the model during recirculation of water in the flume was used as indicator of flow direction. The streamline patterns that Allen obtained from his experiments represent "temporal average" (i.e. mean) of the condition of quasi-steady flows, which makes it comparable with natural flows (see more details in chapter 9 of Allen, 1968). These particular experiments only show the effects of the basal part of sediment-less flows, and their results show good agreement with the interpretation of reversely-oriented imbrication caused by the shear-stress of basal backflows over the lee-side of the dune-like deposit of Sequence 3.

6.5.1 Applicability of laboratory models: kinematic and geometrical similarity

The comparative analysis of the sedimentary architecture of Sequence 3 with the experimental models of Allen takes into account the three main types of similarity for the analysis of fluid mechanics: geometry, kinetic and dynamic (Albertson et al., 1960). Experimental models provide data with respect to the dimensions of the model (geometry), pattern of motion of a fluid (kinetic) and flow physical properties in the form of dimensional numbers (dynamic). The aim of the comparative analysis is to use this principle of similarity to propose a model that explains, as much as possible, the hydrodynamics of the process that formed the Guredin palaeo-bedforms.

The interpretation of a 'perfect' crescent-shaped scour from the geometry of the lower bounding surface of Sequence 3 (see stages 5 and 6 of Figure 11) makes possible to establish a geometrical similarity with models of Allen's flume experiments (1968). A dynamic similarity cannot be tested since it was obviously not possible to measure any of the physical properties of the palaeo-flows responsible of the either the crescent-shaped scour or the deposits of Sequence 3 (e.g. flow depth and velocity). In any case, flow parameters of Allen's flume experiments and those responsible of the Guredin bedforms are surely in a scale rage not comparable. On the other hand, a kinematic similarity can partially be defined using data collected from the sedimentary architecture of Sequence 3 (i.e. palaeocurrent directions from clast imbrication, clast-size distribution and the reconstructed dune-like morphology).

The model of Allen that best fit a real-world crescent-shaped scour consists of two equally handed-step elements joined together, with downstream angle of closure of 120˚ ('reverse closure negative step')

538 and a riser with an angle of dip of 30˚ and a constant height of ~2.5 cm (see to the left of Figure 13).
539 This model is the best analogue to the interpreted crescent-shaped scour in Sequence 1 and 3, whose
540 chutes, interpreted from the lower bounding surface of Sequence 3, have an angle of dip of ~30˚ (Figure
541 5). Allen did not make more than one model of a reverse closure negative step with an inclined riser, so
542 it has been not possible to compare similar settings (i.e. an angle of closure with a different value or,
543 more appropriately, a perfect crescentic morphology). He did two runs in this model with different step
544 and flow height relations (H/d) and Froude number (F): the first, H/d= 0.16 and F=0.38; the second
545 H/d=0.48 and F=0.77. Allen's model yielded in both runs an almost exact streamline pattern (see Allen,
546 1968). The area of the riser of the step of Allen's model shows a streamline pattern with a convergent
547 pattern of backflows (see left sketch of Figure 13). This convergent streamlines correspond to the lower
548 part of the separation bubble that forms by the entry of subcritical sediment-less flows on a step (Allen,
549 1968). One critical question is if the sediment-laden flow that formed the dune-like deposit of Sequence
550 3 could have developed a similar streamline field assuming a crescentic shape for the scour. The
551 answer is here not possible to be convincingly answered but the imbrication measured on the dune-like
552 deposit of Sequence 3 can be a lead.

553 The imbrication observed on Sequence 3 is here interpreted to have developed during the progradation
554 of the lee-side of a dune-like deposit. The divergent directions obtained from the measured dip
555 directions of imbricated clasts (Figure 12) would yield a convergent streamline pattern assuming they
556 are regularly-oriented (i.e. interpreting a palaeocurrent direction opposite to the downslope direction of
557 the a-b plane of imbricated clasts). This convergent pattern has been drawn on a sketch analogue of
558 that of the flume model of Allen that shows an intermediate stage during the formation of the dune-like
559 deposit of Sequence 3 into a perfect crescent-shaped scour (see sketch to the right in Figure 13). Let's
560 assume that a kinematical similarity between a data from a flume model and field data can be
561 extrapolated to a geometrical similarity. If the two risers of the reverse closure negative step of Allen's
562 model yield a convergent pattern of basal flows as part of a separation bubble, the similar pattern
563 obtained from the imbrication data on the lee-side of the dune-like deposits of Sequence 3 can suggest
564 a concave downstream morphology (see the concave downstream dotted red line in the sketch to the
565 right of Figure 13). Does this mean that the entry of the sediment-laden flow into the interpreted
566 crescent-shaped developed a separation bubble with a convergent pattern of backflows from the very
567 start and maintained it during the formation of the dune-like deposit? An affirmative answer would

assume that streamline fields obtained from experiments with sediment-less flows are similar to those with sediment-laden flows (at least basal flows).

The uncertainty on the interpretations considered so far could be minimised by further experimentation with sediment-laden flows that develop separation zones in scours analogue of those observed on modern submarine channels. It would be interesting to test what would be the streamline field developed by sediment-laden flows entering scours with variations in key their geometrical attributes (e.g. the planform curvature of the crescentic step and the slope gradient of their lee- and stoss sides).

6.5.2 Streamline field in a crescent-shaped scour developed by the entry of a dense basal subcritical flow

What would be the pathways and areas of deposition of clasts that enter a separation bubble developed into a crescent-shaped scour? Results from the experiments of Allen (1968) make possible the construction of a streamline field model for a crescent-shaped scour during the entry of subcritical sediment-less flows. As one of Allen's models is geometrically similar to the palaeo-scour interpreted for the deposition of Sequence 3, it is possible to compare streamline patterns observed and inferred in each case respectively. This comparison shows agreements in these patterns and can largely explain the complete sedimentary architecture of Sequence 3 (including the reconstructed dune-like geometry of the resultant palaeo-bedform).

The main hydrodynamic phenomenon that results from the entry of a subcritical flow in a scour is a flow separation, and one of the main zones resultant of this phenomenon is the separation bubble (see the downstream section of a flow separation through the central part of a crescent-shaped scour in sketch 'B' of Figure 14). Allen (1968) observed that the strength of separation bubbles (i.e. velocity) changes according to the angle of skew of the steps of each of the constructed models with respect to the direction of the entry flow (i.e. the angle of attack). The angle of attack of subcritical flows over steps with different angle of skew not only controls the strength but the configuration of the streamline field. Allen distinguished two types of separation bubble configurations depending on the morphology of the separation surface (Allen, 1970): rollers and vortices. Rollers develop closed separation bubbles and vortices open bubbles with respect to the outer stream (which starts from reattachment lines; see sketch 'C' of Figure 14). Allen also observed that rollers occur when the angle of attack of flows over the edge

596 of the step is in the range 90˚ to 45˚ whereas vortices form in the range 45˚ to 0˚ (notice that Allen,
597 1968, used a nominal angle of skew of 180˚ instead of 90˚ for each side).

598 The results of Allen's (1968) experiments with different angle of skew of steps can be used to
599 reconstruct the streamline field of an infinite variety of planform morphologies of scours. The drawing of
600 a curve integrating all the possible angles of attack along a downstream direction (from 90˚ to 0˚
601 towards both sides of a given point) will render a convenient crescentic morphology (see the example of
602 sketch 'A' of Figure 14). Any possible conic section shape with an analogue crescentic form can be
603 produced changing the rate of angle of attack versus downstream total distance of this shape. Adjusting
604 a crescentic shape to any possible conic section, the angle of attack will always increase from the
605 inflexion point towards both sides of the curve (stating always from an angle of 90º to a minimum of 0º;
606 see the encircled point 'S' in sketch 'A' of Figure 14). At a given point both sides of the curve will reach a
607 value for the angle of attack of 45˚, which is the threshold for the development of either rollers or
608 vortices in the separation bubble. The sketch 'A' of Figure 14 depicts an example of a given crescent-
609 shaped scour whose streamline field only shows backflows at the lower part of the separation bubble
610 (see white arrowheads).

611 One of the key questions is if streamline field models from sediment-less flows can be applied in
612 sediment-laden ones. If that is the case, kinematic models for crescent-shaped scours can be used to
613 infer the average pathway of clasts upon the entry of subcritical sediment-laden flows. The development
614 of rollers and vortices appear to be the key for the prediction of the final sedimentary architecture of the
615 scour-fill. The pathways between rollers and vortices are remarkably different, which is expected to
616 impact on the final sedimentary architecture of the resultant deposit. Rollers are totally closed
617 separation bubbles where the lower streamlines are backflows redirecting the clasts towards the lee-
618 side of the step (see sketch 'C' in Figure 14). The location of rollers in the central part of a crescent-
619 shaped scour would explain why the pervasive imbrication was only found in a similar area for the
620 interpreted concave downstream lee-side of the dune-like deposit of Sequence 3 (i.e. the axis area of
621 the strike-cross section of the dune-like deposit; see Figure 12). On the other hand, the areas to the
622 sides of the initial crescent-shaped step would have been controlled by vortices. These vortices are
623 partially closed separation bubbles that would have driven clasts towards each of the downstream ends
624 of the scour (see sketch 'C' in Figure 14). In this case, the shear stress imparted by flows on the lee-

side would have yielded imbrication patterns that would suggest directions veering from perpendicular to slightly oblique with respect to the downstream mean direction of the subcritical flow. These palaeocurrent directions were not observed in Sequence 3. As the data from the Guredin palaeo-bedforms was collected before the present streamline model was envisaged, fieldwork was not planned to test this model. It cannot be discarded the existence of unnoticed imbrication showing these oblique directions at the northern margin of the strike-section of Sequence 3 (i.e. next to point 'F' Figure 7 and Figure 12).

6.5.3 A hyperconcentrated flow with a basal traction carpet

Certain observations from experiments with turbulent half-jets loaded with sediment appear to be compatible with observations on the clast-size distribution of Sequence 3. Allen (1965) and Jopling (1964, 1965) focused on the path of grains upon their entry into steps (a two-dimensional analysis through downstream sections). They suggested that starting velocity vs free falling velocity ratio (i.e. the dimensionless starting velocity) and the height with respect the edge of the step is fundamental in their final area of deposition of grains. In general, the larger is the ratio and the higher is the position of grains, the farther (along the flow direction) and more dispersed is the area of deposition. Allen's (1968) experiments were more complete and thoroughly controlling the effect of each of these and other variables (e.g. grain size). He confirmed the former effects of variables and stated that diffusion of grains in the spatially growing vortices of the free boundary layer in a flow separation is probably a dominant process in the spatial distribution of clasts over the lee-side of a step and beyond.

When Allen (1965) used relatively poorly sorted sand in a set of his experiments (unlike Jopling's experiments), he observed that the coarsest grains would settle roughly mid-way between the edge and the bottom of the lee-side or riser. Allen (1965) argued that the differential distribution of clast sizes that he observed could occur because of a basal flow with inverse vertical distribution of clast-size (neither Allen not Jopling's experiments could control the velocity, concentration, and size distribution in the bedload so to define the type of basal flow structure and transport mechanisms in detail). He linked this hypothesis with the inverse graded turbidites described by Walker (1965) and a sorting mechanism controlled by the dispersive pressure in the bed layer defined by Bagnold (1954). This type of flow structure matches the description of a 'traction carpet' at the lowermost part of a 'high-density turbidity current or flow' (Lowe, 1982).

654 The expected inverse graded facies of traction carpets can be explained by other processes apart from
655 dispersive pressure, like kinetic sieving (Middleton, 1970) and depletive waxing flows (Kneller, 1995). In
656 the case of the predominant low-angle cross-bedded amalgamated conglomeratic sandstones of the
657 CS3 canyon-fill, it is preferred the interpretation of traction carpets based on the process description of
658 Sohn (1997) where dispersive pressure causes inverse grading. Firstly, the facies descriptions of these
659 deposits largely fit in Sohn's facies types for traction carpets. Secondly, the analysis of maximum clast
660 size data over a ~200 m long section of the CS3 canyon-fill supports the progressive preservation of the
661 complete flow structure of the traction carpet as the canyon was being filled (see Lopez Jimenez, 2017).
662 The preservation of the flow structure of the traction carpets on the outcrop can be explained by either
663 the "sudden 'freezing' of the flow" as a consequence of the driving gravity stress overcoming the yield
664 strength of the sediment (Middleton and Hampton, 1973) or the continuous aggradation of the layers
665 that comprise the 'carpet' structure (Sohn, 1997). The presence of facies preserved from traction carpet
666 transport mechanisms would point to either hyperconcentrated or concentrated density-flows as per the
667 classification of see Mulder and Alexander (2001). In the particular case of the flows responsible for the
668 Guredin palaeo-bedforms, the definition of hyperconcentrated flows suit better for the following reasons:
669 1) the predominant amalgamated character in the conglomeratic deposits of the CS3 canyon-fill (with
670 scarce presence palaeo-scours) supports the interpretation of a liquefaction process with associated
671 hydroplaning where basal gravelly sands moved at relatively high-velocity but causing little erosion to
672 the substrate; 2) the presence of boulder-size clasts in the sedimentary architecture of the Guredin
673 palaeo-bedforms (i.e. Sequence 3), which can be transported by the aforementioned liquefaction
674 process or just by the upward force imparted by grain-to-grain collision.

675 Let's take the structure of a traction carpet as part of a hyperconcentrated flow into the two-dimensional
676 analyses of Allen's experiments (1965, 1968) and compare it with the observed clast-size distribution of
677 Sequence 3 on the exposed downslope section (see sketch 'D' in Figure 14). As the downslope section
678 of Sequence 3 is close to the inflexion point of the reconstructed crescent shape of the paleo-scour (see
679 Figure 12), the angle of attack of the flow would have had a value close to 90º. Thus, this section is
680 analogue to flume settings of Allen (1965, 1968) where grains were injected perpendicularly to a straight
681 step. A traction carpet entering the crescent-shaped scour would have comprised of a zone dominated
682 by boulder-size clasts (since clasts with this size are part of Sequence 3). In a traction carpet with
683 effecting dispersive intergranular pressure, the boulder zone would have been located in a roughly

middle position of a vertical section of the basal flow structure. Cobbly-pebbly sandstones would have dominated the zone beneath the boulder zone. Assuming the height and starting velocity as major controlling factors of the clast paths-lengths, cobbly-pebbly sandstones would have settled in the most proximal and higher part of the lee-side of the scour (see blue pathway in the sketch 'D' in Figure 14). Boulders, located at a higher position, with a higher starting velocity but also free falling velocity would have been deposited in an area immediately further downstream (in a roughly middle reach of the lee-side of the step and probably beyond; see magenta pathway in the sketch 'D' in Figure 14). This description is similar to that of Allen (1965, Chapter 6) over straight steps and agrees the sedimentary architecture of the downslope section of Sequence 3: all the observed boulders are located at the middle zone of this section (see the reconstructed complete downslope section in the sketch 'D' of Figure 14).

Another process worth to take into account is avalanching. Avalanching was observed and analysed by both Allen (1965) and Jopling (1964, 1965) during the construction of two-dimensional sand bodies in their experiments (the former focused on reproducing ripples and the latter on deltas). The inference of avalanching was defined by these experimentalists as the creation of foresets with a 3D tongue-like morphology where the clast-size increases in a downslope direction (i.e. the coarsest clasts concentrate at the periphery of the tongue, located in the lowest position of the deposit). This characteristic was observed to change when the sediment discharge was increased, with the consequence of the increase of avalanching frequency (Jopling, 1965 and Allen, 1965). This situation would not make possible effective grain sorting processes during each avalanche (e.g. dispersive intergranular pressure), resulting in the concentration of the larger clasts at near the edge of the step. None of these scenarios is the case for Sequence 3 since the coarsest clasts (boulders) are located in the core of Sequence 3 (i.e. the central part of the complete scour-fill deposit) but not towards the margins. Avalanches would have transported boulders also towards both sides of the scour-fill (following the tongue-like deposit formation). The only discrete beds that might be interpreted as avalanching facies are the observed cobbly clast-supported stripes (see Figure 10 and Figure 12). As these beds or stripes are an anomaly to the concentric clast-size distribution of Sequence 3, they might have been result of sideways avalanches from areas located at the centre of an already forming dune-like bedform (where cobbles where being preferentially deposited). Another critical observation is that the observed pervasive imbrication is continuous across these coarser-grain stripes. The process associated with this

imbrication appears to have been operating continuously and with the same effect on the clast orientation even during the deposition of any potential avalanche. In summary, the interpretation of avalanching is not clear from the observations on the sedimentary architecture of the Guredin palaeo-bedforms. Allen's experiments made him realise that "at high sediment discharges, avalanching ceases to be a significant mechanism of grain sorting and emplacement on the leeside". The palaeo-flows responsible of the formation of Sequence 3 could have had this relatively high sediment discharges.

6.5.4 A model for the development of dune-like deposits into crescent-shaped scours

Allen's (1968) experiments revealed that the variables controlling the clast path-lengths from turbulent half-jets can be more complex than the height and starting velocities (e.g. streamline directions or turbulence in different parts of the separation flow, and effects of the clast concentration on the clast settling velocity). Besides, Jopling's and Allen's experiments were either two-dimensional or 3D but with geometries far simple than that of a crescent-shaped scour. Actually, Allen (1968) observed that when grains are diffused over oblique steps (i.e. 30º and 60º) the area of deposition of grains appeared to be affected by the structure of the separation bubble. His research was focused on ripples, but his findings help to interpret the dynamics of the flows responsible of the Guredin palaeo-bedforms. The integration of the model of the streamline pattern of a generic crescent-shaped scour (Figure 14) with all the above explained theory of clast path-lengths in the downstream section of a separation bubble can satisfactorily explain the particular sedimentary architecture of the dune-like deposit of Sequence 3. The first key aspect is the presence of the core consisting of clast-supported cobbly sandstone with imbrication patterns indicating backflows. This core would be result of the trapping of the part of the hyperconcentrated basal flow with the largest clasts that would fall into a roller. The roller would have acted as a trapping mechanism since the comparatively low velocity of backflows could not transfer them further downstream (see Stage 2 in Figure 15). The central part of the separation bubble, with a major roller stretching from the lee-side of the step to the reattachment line, could be envisaged as a 'centrifugation mechanism' that would efficiently separate clasts according to their weight and shape. This centrifugation mechanism would explain the more clast-supported character of the cobbly sandstones located at the central part of the interpreted crescent-shaped scour (Figure 9). The second key aspect of the architecture of Sequence 3 is the dune-like morphology defined by its upper bounding surface. This dune-like morphology is depicted as a central crest that rapidly wedges out sideways (see

Figure 12). The crest can certainly grow by the continuous settling of the coarsest clasts of the dense basal flow and maintain its structure by the shear-stress of backflows of the separation bubble (i.e. vortex). Conversely, the general downslope transfer of sediment at both sides of the crescent-shaped scour would fit with the development of wedged-shape margins in the dune-like deposit of Sequence 3. Most of the largest clasts of the basal flow entering the vortices at the edges of the crescent-shaped scour would have bypassed beyond the crescent-shaped scour (see Stage 2 in Figure 15). As Allen (1968) found, the vortices yield clast pathways with stronger downstream velocities the lower is the angle of attack (i.e. to the margin ends of the crescent-shaped scour). Therefore, it can be suggested that the margins of the deposit filling the crescent-shaped scour would have a downstream wedge-shape in planform view (e.g. similar to a barchan dune; see Stage 3 of Figure 15).

The interpretation of the bedform resultant from the complete constructional process here described is summarised in Figure 15. This integrates the erosional process associated with a hydraulic jump that formed the crescent-shaped scour (stage 1, supercritical flow) and the formation of the dune-like deposit of Sequence 3 during the entry of hyperconcentrated flow with a traction carpet basal structure into a separation bubble (stage 2, subcritical flow). The final planform morphology of the deposit filling the crescent-shaped scour can entail further speculation (stage 3). The barchan morphology is intuitively more likely considering the proposed self-maintained streamline model in a crescent-shaped scour with rollers and vortices. However, other downstream planform morphologies cannot be ruled out, especially from observations in modern submarine channels (see different possible downstream terminations of the resultant bedform on the sketch to the right of Stage 3 in Figure 15).

6.6 Comparison with analogues in modern submarine channels

The interpreted dune-like deposit with a concave-down lee-side formed into a crescent-shaped scour (see Figure 15) is a bedform type that can partially be recognised in the Monterey Canyon (which gravelly sands make it analogue to the CS3 Canyon-fill). Surveys in the modern Monterey Canyon stand as the only source of data sets comparable to the sedimentary architecture of the Guredin palaeo-bedforms. Different surveys in this canyon have provided evidence of relatively high-relief bedforms with crescentic morphologies consisting of gravelly sands (Paull, 2010, 2011; Smith et al., 2005, 2007). Paull et al. (2011) differentiated two main of bedforms with respect to their planform morphology: crescent-shaped and reverse curvature bedforms (analogues of Allen's, 1968, reverse closure and forward

772 closure steps, respectively). Figure 16 uses a published bathymetric data set of crescent-shaped
773 bedforms of the Monterey Canyon (Paull et al., 2010). The comparative analysis explained below
774 supports the inference of a constructional process partially based on the model that integrates results
775 from Allen's experiments with the analysis of the sedimentary architecture of the Guredin palaeo-
776 bedforms.

777 The top of Figure 16 shows a bathymetric map of a section of the Monterey Canyon where its width is ~
778 200 m (modified from Paull et al., 2010). The crescentic edges of the lee-side of steps as well as the
779 relative bathymetric highs and lows are highlighted in purple, red and green respectively (only highs and
780 lows located in central or axial parts of the bedforms are highlighted). The selected area shows a train
781 of crescentic steps whose margins (i.e. lateral ends that meet the either the canyon or a terrace) join to
782 the next one in a downstream direction. The width of the crescentic edges are similar to the interpreted
783 crescentic-shaped associated with Sequence 3 (~150 m wide). Conversely, the Guredin palaeo-
784 bedforms are in a canyon ~2.5 km wide and located ~300 m from the north-western canyon-wall (see
785 Figure 2). The height of the lee-side of the steps is difficult to assess in the case of the Guredin palaeo-
786 bedforms. However, the deposit of Sequence 1 suggest a step of ~5 m high (see Stage 3 in Figure 11),
787 which is similar to the range of 2-4 m for the lees-side heights of the Monterey bedforms indicated in
788 section A-A' of Figure 16.

789 The absence of internal reflections on chirp seismic profiles from surveyed gravelly sand bedforms of
790 the Monterey Canyon can preliminary be interpreted as a disorganised internal architecture (Paull et al.,
791 2010, 2011). However, the contrast impedance in a deposit without discrete beds consisting of very
792 different clast-size classes (i.e. Sequence 3) is a good candidate for rendering such apparent
793 disorganised internal architecture. This means that a deposit consisting of zones with different average
794 clast-sizes is possible in these apparently disorganised deposits. Moreover, it can be extracted a
795 fundamental similarity between the Monterey Canyon and the Guredin case studies combining the data
796 sets of bathymetric sections and vibracores from Paull et al. (2010): gravel-size clasts concentrate at
797 the area around the inflexion point of the crescentic lee-side of the steps. The bathymetric profiles of
798 Figure 16 (labelled A-A' and B-B') indicate where these concentrations of gravelly deposits were found.
799 The length of vibracores ranged from 0.50 to 1.90 m and they were drilled along the tracks of the
800 bathymetric sections. These vibracores show gravelly sands concentrated on the lee-sides of steps and

on the relative bathymetric highs located a few metres upstream of the edges of each step (encircled in red in the bathymetric map of Figure 16). These bathymetric highs confer a dune-like morphology (through strike-cross sections) to the deposits constrained between two contiguous crescentic steps (see annotation in B-B' section of Figure 16). These observations coincide with the described core at axis of the dune-like deposit of Sequence 3 consisting of a greater concentration of the largest clasts (i.e. the clast-supported cobbly sandstone with occasional boulders zone shown in the strike-cross section of Figure 12). If a similar concentric zonation of clast-size classes is interpreted in the dune-like morphologies of deposits between crescentic steps of the Monterey data set, is it possible to also suggest a depositional mechanism controlled by a separation bubble?

The Monterey and the Guredin palaeo-bedforms fit in the type defined by Symons et al. (2016) as 'small-scale sediment waves with mixed relief in confined settings and small-scale systems'. Symons et al. (2016) do not use the relief as discriminator for classifying bedforms since they cannot use either the crescentic planform or the cross-sectional morphologies useful for classifying bedform types. However, the constructional process described for the sedimentary architecture of Sequence 3 points to an important relationship between the complete 3D morphology of bedforms and their constructional processes. The bottom of Figure 16 shows the reconstruction of the complete 3D morphology of, first, two consecutive crescent-shaped bedforms of the selected bathymetric data set from the Monterey canyon, and second, the bedform resultant from the deposition of the dune-like deposit of Sequence 3 into a generic crescent-shaped scour. The key difference between both reconstructions is the relative low-relief located by the central part of the lee-side of the step. This is present in the Monterey Canyon bedforms but absent in the case of the Guredin palaeo-bedforms (not only in the palaeo-bedform associated with Sequence 3 but also in case of Sequence 1). It is clear from Figure 5 that the depositional process of the dune-like deposit associated with Sequence 3 created a ramp from the edge of the central part of the crescent-shaped scour towards a position downstream. If hyperconcentrated basal flows deposited its load controlled by a separation bubble in the selected crescent-shaped bedforms of the Monterey Canyon, how these bathymetric highs and lows can be explained with regard to this process? If erosional hydraulic jumps are involved in the formation of the bathymetric lows, what is their role in the construction of the dune-like morphology and the core of gravelly sands?

It is important to notice that the bedform associated with Sequence 3 of the Guredin palaeo-bedforms is preliminary interpreted to have existed as a relatively isolated individual in a comparatively large canyon. However, probably other similar bedforms formed in areas both up- and downstream since other dune-like bedforms have been found in a downstream position of the CS3 canyon-fill (see Figure 2 and Figure 3). Conversely, the Monterey Canyon bedforms are a sequence of several individuals (a 'train' of bedforms) that stretch across most of the canyon-width. Considering that changes in channel morphology and flow physical properties constitute a feedback process, how much a dimensional relationship between the crescent-shaped bedforms and the canyon morphology is responsible of variations of the constructional process described for Sequence 3?

In the case of the Monterey bedforms here analysed, there is not enough data from their internal structure to determine a relationship between bedform, internal sedimentary architecture and their interpreted constructional process. However, there is other data and observations from surveys that add valuable information for a discussion on the constructional process. The Monterey bedforms are known to maintain their general crescentic morphology after several sediment-laden flow events (Paull et al., 2010). 'Fluidized movement of sediment' has first been hypothesised to occur from the movement of deployed monuments (Paull et al., 2010), which have later been supported by data from surveys in areas of the Monterey Canyon where crescent-shaped bedforms occur (Coordinated Canyon Experiment, 2018). The inference of this type of flow fits with a hyperconcentrated basal flow type (*sensu* Mulder and Alexander, 2001). The constructional process of these bedforms involving such type of basal flows has been found incompatible with the cyclic step paradigm (Paull et al. (2011). The constructional process here defined for the Guredin palaeo-bedforms is able to explain a constructional process different from the cyclic step paradigm by the entry of hyperconcentrated flows in a probable subcritical regime into crescent-shaped scours. As this model is speculative, it does not intend to give a unique final solution for the construction of relatively high-relief crescent-shaped bedforms consisting of gravelly sands, but to show new research paths for their complete understanding.

6.7 Uncertainty in the definition of the structure of flow events

Relatively high-relief crescent-shaped bedforms are here interpreted to have been formed by a two-stage process consisting of the formation of a crescent-shaped scour by a hydraulic jump associated with the change from a supercritical to a subcritical flow regime, and the formation of a dune-like deposit

by a hyperconcentrated basal flow that developed a separation flow (probably in a subcritical regime). This process can be interpreted as part of a complete single flow event assuming a transition from relatively high velocity flows loaded with pebbly sand basal flows to relatively low velocity flows loaded with cobbly-bouldery sands. This flow structure is similar to flows reproduced in laboratory by Postma et al., 1988 and to the model suggested by Azpiroz et al. (2017) for flow events in the Congo Canyon (although with sand to mud-laden flows). This would suggest that gravelly sand-laden flows develop more complex flow transformations compared to fine-grained flows, involving a constructional process and producing sedimentary architectures remarkably different from any of those described for cyclic steps (i.e. upstream bed configurations). Notwithstanding, as the timing of the deposition of the sequences of the Guredin palaeo-bedforms cannot be reliably determined, it is not possible to clearly differentiate flow events from the present ancient outcrop case study.

6.8 Implications in classification schemes of bedform types

The sedimentary architectures and model of constructional process here proposed for a relatively high-relief crescent-shaped bedform would imply a modification on proposed classifications of seafloor bedforms (e.g. Cartigny et al., 2014; Symons et al., 2016). How would be classified a bedform on a submarine channel resulting from a process define as follows: the formation of a net-erosional cyclic step (a crescent-shaped scour in 3D) upon an abrupt change from super- to subcritical flow regime, followed by the formation of a dune-like deposit from the entry of a subcritical flow with a hyperconcentrated basal phase? Using a classic stability diagram with bedforms that form in different flow regimes, the high-relief dune-like bedform of Sequence 3 can be described by the transition from the cyclic step field to another field in the subcritical regime (aka ‘two-regime transition bedform’). None of the bedform types described in the subcritical regime these stability diagrams satisfy the formation of the dune-like bedform of Sequence 3. The definition of classic dunes by free-surface air-to-water flows differ markedly from that of the dune-like deposit into a crescent-scour by a subcritical flow. Gravel dunes have been explained as consequence of free-surface subcritical flows (Carling, 1999) and they are included in stability diagrams for ‘turbidity currents’ (Cantigny and Postma, 2016). Thus, ‘true’ dunes and dune-like bedforms are constructed by subcritical flows but from different initial conditions (i.e. substrate morphology) as well as by flows with potential different dynamics and structure (in particular for the dense basal part of flows, whose description is largely hypothetical; see Mulder and Alexander,

2001). It is always important to be aware that gravity-driven sediment-laden flows are prompted by the movement of clastics by the gravity field, whereas in free-surface air-to-water flows the interstitial fluid, water, is moved by the gravity field and might move clastics within it. All of these differences bring up a series of questions that has an impact on the creation of a classifications for gravity-driven sediment-laden flows: if the dune field of stability diagrams cannot be used for the here described dune-like bedforms, what would be the name and the process that defines them?, what other combinations of changes in the regime of gravity-driven sediment-laden flows can occur in submarine channels? What is the effect of the different types transport mechanisms in these types of flows that interact with scours? How to include the role of 3D streamline fields associated with particular seafloor morphologies in stability diagrams? And the final question, what are all the possible resultant bedforms from all these combinations of regime changes, seafloor morphologies plus dynamics and structure of flows?

The timing of occurrence of the phases of described for the flow event interpreted for the sedimentary architecture of Sequence 3 is here suggested as likely to occur in modern submarine channels transporting gravelly sands. Surveys in modern submarine channels have provided data that has been interpreted in the form of contrasting models of flow event structures (e.g. Sumner and Paull, 2014; Symons et al., 2017). These models do not describe the relatively complex flow structure here described for the Guredin palaeo-bedforms. This should not invalid the model here proposed since these models correspond to particular cases of flow events in relatively limited channel reaches and transporting comparatively fine grained sediment.

It is critical to be aware that, as in the case of the Guredin palaeo-bedforms, a bedform that is observed in modern channels can be result of unsteady and non-uniform sediment-laden flows that interact changing substrate morphology. Future studies in modern environments (e.g. Coordinated Canyon Experiment, 2018) combined with more studies like the present one in ancient outcrops can provide data for creating complete stability diagrams and a bedform classification for gravity-driven sediment-laden flows. This completeness will overcome current classifications large limited to the bedform morphology where the role of subcritical flow phases is not considered and the internal sedimentary architecture of the deposit associated with that bedform cannot be described in detail (e.g. Symons et al., 2016). The study of the other palaeo-bedforms already found in the gravelly sandstone deposits of

915 the channel-fills of the Alikayasi system are expected to add support to the hypotheses discussed in the
916 present study and provide more insights on the understanding of gravity-driven sediment-laden flows.

917 7 Conclusions

918 The analysis of the sedimentary architecture of the Guredin palaeo-bedforms shows evidence for a
919 constructional process of relatively high-relief crescent-shaped bedforms not related to the cyclic step
920 paradigm.

921 The process is explained by the occurrence of two distinctive phases during a flow event. The first flow
922 phase produces a crescent-shaped scour and the second a dune-like deposit inside the former. This
923 phase is defined by a supercritical flow that develops an erosional hydraulic jump (responsible of the
924 formation of the crescent-shaped scour) as it changes abruptly to a subcritical regime. The second
925 phase is defined by a subcritical flow with a hyperconcentrated basal flow that, upon its entry in the
926 scour, develops rollers and vortices as part of a separation bubble. The resultant streamline field
927 developed in the crescent-shaped scour can be predicted and it is suggested to be responsible of the
928 formation of the observed dune-like geometry of one of the scour-fill deposits. The formation of the
929 dune-like deposit entirely depends on the previous formation of the crescent-shaped scour but probably
930 also on the entry of a hyperconcentrated flow with a basal traction carpet structure.

931 This constructional process finds partial support from the integration of the following data set: field-
932 based evidence (from an ancient submarine canyon-fill), published results on experimental modelling
933 (from subcritical flows bypassing steps) and data sets from a modern submarine canyon (the Monterey
934 Canyon). This integration shows agreement to a large extent but also differences. The differences open
935 a series of questions on the possible range of variations of this constructional process that can occur in
936 real-world settings.

937 The Guredin palaeo-bedforms is a unique case study that needs further support from modern and other
938 ancient case studies. However, this work points to the rethinking of proposed classification schemes
939 and constructional process models for high-relief bedforms related to gravelly sand flows.

940 The analysis of the Guredin palaeo-bedforms highlights the value of data from ancient outcrop case
941 studies for the understanding of the physical properties of flows in the submarine environment and their

consequences on the seafloor. The continuation of collection of data from other outcrops of palaeo-bedforms in the Alikayasi system (and other ancient case studies) will contribute to the understanding of the hydrodynamics of gravelly-sand laden flows and their consequences on the seafloor.

8 Acknowledgments

Despite this research was self-funded, the Guredin palaeo-bedforms were discovered during the doctoral studies of the author (as part of the Turbidites Research Group at University of Aberdeen; the PRACSS consortium project). The author thanks Colin Turner for his review of an earlier version of the manuscript. He also expresses his gratitude to George Postma and Matthieu Cartigny for their reviews and discussions. This author is especially grateful to Ahmet Özer for providing of accommodation and company during fieldwork.

9 Figure captions

Figure 1 – Geographic map with major regional tectonic structures showing the localisation of the Maras Basin in the south of Turkey. This geographic map shows Turkey on the centre (light grey lines are country boundaries) plus tectonic plate boundaries of in the region. The main plates in this region are the African Plate (AFP), the Arabian Plate (ARP), the Anatolian Microplate (ANP), the Aegean Microplate (AGP) and the Eurasian Plate (EAP). The main regional tectonic structures are the Dead Sea Fault Zone (DSFZ), the East Anatolian Fault Zone (EAFZ), the Bitlis-Zagros Suture Zone (BZSZ), the North Anatolian Fault Zone (NAFZ), the Cyprean Arc (CA), the Aegean Arc (AA), the Mediterranean Ridge (MR) and the Florence Rise (FR). A yellow star shows the location of the Province of Kahramanmaras where the Miocene Maras Basin crops out (in a triple tectonic junction).

Figure 2 – Satellite view of the northernmost part of the Alikayasi System (the oldest deposits). This Google Earth view shows the extension of coarse-grained deposits (conglomerates and sandstone) that constitute the sedimentary architecture of channel-fills of the Alikayasi system (shaded areas). The greenish shaded areas bounded by red lines constrain deposits of the CS3 Canyon. Yellow camera miniature indicates photoshoot locations of two panoramas shown in Figure 3 (P1) and Figure 5 (P2). The Guredin palaeo-bedforms crop out at P1. The yellow star indicates the location of other similar palaeo-bedforms. The yellow arrow indicates the palaeocurrent exclusively for the CS3 canyon-fill

deposits (ENE to WSW). The value 'Dip~15°' indicates angle of dip of the CS3 canyon-fill deposits to the WSW (i.e. the direction it continues in the subsurface). Both palaeocurrent and dip directions of channel fill deposits were measured on sole marks.

Figure 3 – Panorama and photo-interpretation of a strike section of the CS3 Canyon-fill. The panorama at the top was taken from the P1 photoshoot location (above the outcrop of the Guredin palaeo-bedforms). The bottom photo-interpretation shows a complete reconstruction of the architectural framework (i.e. main bounding surfaces) of the CS3 canyon-fill (including the eroded NW margin). The architectural framework of the CS3 canyon-fill is defined as follows: 1) a first order bounding surface (red line) shows the maximum bathymetric aspect that the palaeo-canyon could develop; and 2) second order bounding surfaces constraining a vertical stack of three filling phases that stretch across the entire concave-up space of the palaeo-canyon. The three filling phases are connected at their central parts and each of them wedge out to the margins. The filling phases consist of conglomeratic sandstones, dominated by matrix-supported pebbly sandstones with low-angle bed configurations. This predominance is broken by areas constrained to the north-west margin of the third filling phase, where there are outcrops of relatively high-angle cross-bedded cobbly sandstones with occasional boulders. These outcrops include the Guredin palaeo-bedforms, and others found further to the south-west (see yellow star). Wedges consisting of heterogeneous facies (mixed conglomerates, sandstone siltstone and mudstone) interfinger the space left by the margins of the filling phases.

Figure 4 – Low-level satellite image of the outcrop of the Guredin palaeo-bedforms at the Guredinkalesi hill. The orange shaded area constrains the deposits of the Guredin palaeo-bedforms (as shown on Figure 5). The encircled letters are spatial reference points used in following figures. Black rectangles with numbers intersecting with lines indicate the extent of main sections with particular orientations, relevant for the description of the sedimentary architecture of the Guredin palaeo-bedforms. P1 is the exact photo-shoot location also shown in Figure 2. The norther limit of the deposits that overlain the Guredin palaeo-bedforms describes a lineation with an arcuate geometry that is here related to a palaeo-surface of a bedform (white dashed line).

Figure 5 – Panorama of the Guredin palaeo-bedforms at the Guredinkalesi hill. This panorama shows a general view of the exposures of the Guredin palaeo-bedforms at the Guredinkalesi hill (the photo-shoot location is labelled P2 in Figure 2). Three sequences (with different colours) define the

deposits associated with the palaeo-bedforms that developed in the relatively flat floor of the CS3 Canyon (notice the parallel bed configuration described by thin black lines in blank areas). These sequences are constrained by major bounding surfaces (thick black lines). Encircled letters serve as reference points (as also shown on Figure 4). Several of these points define the extension of key exposures with variable orientation (see black rectangles with numbers from 1 to 3). The lower bounding surfaces of Sequences 1 and 3 are overlain by deposits with comparatively large average clasts-sizes.

Figure 6 – Photo and interpretation of a strike cross-section of Sequence 1 and 2. The bottom photo-interpretation shows the highly eroded, concave-up morphology of lower bounding surface of Sequence 1. This surface truncates the previous deposits consisting of the dominant pebbly sandstones of the CS3 Canyon-fill. This view shows relicts of rip-ups of unknown deposits that fell off the exposure. There is a sharp transition from clast-supported pebbly to cobbly deposits at the bottom of Sequence 1, which coincides with the bounding surface of a foreset observed on the downslope section of the same deposit. The uppermost part of Sequence 1 shows a rapid fining to sandstone parallel beds. Patches of deposits from Sequence 2 and 3 are also shown in this figure.

Figure 7 – Photo of the western-most part of the Guredin palaeo-bedforms and results of logs on the lower part of Sequence 3 (see points of reference for location in Figure 5). The shoot location of this photo is ~500 m to the SE of that of P2. White dotted lines show bounding surfaces between sequences. The photo shows the sharp contact between Sequences 1 and Sequences 2 and 3. Part of Sequence 3 truncates Sequence 3 in two separated exposures (indicated with black arrows). Sequence 2 shows a downlapping bed configuration over the contact with Sequence 1. The bedding orientation of the upper bounding surface of Sequence 1 is 080˚/5˚N (see the annotation next to point 'D'). The area labelled S2-1 shows a close-up the Sequence 2 in Figure 8. Sequence 3 shows lineations with an angle of dip of ~50˚ to the WSW consisting of pervasively imbricated clast-supported cobbly sandstones with occasional boulders (see area labelled S3-1 – Figure 9). The area labelled S3-2 (see Figure 10) shows a close-up of pervasively imbricated pebbles and cobbles on the strike cross-section of Sequence 3. The white arrows mark the upper bounding surface this section, which describes concave-upward shape. The coloured vertical lines mark the position of logged sections. The results of these logs are shown at the bottom of the figure. The horizontal axis indicates the value of the maximum clast size (in

cm) measured across 1 m over the exposure every 10 cm along the vertical section. The vertical axis indicates the position over the total length of the logged section. Numbers associated with AVG and MD indicates values for average and mean deviation of all the maximum clast size measurements in each log. The symbol consisting of three ellipses with numbers below indicates measurements of pervasive imbrication. The imbrication defines parallel lineation observed from afar, which are only discernible in the westernmost part of Sequence 3, below reference point 'E' (where boulders are also observed). The first number is the angle of dip and the second the dip direction of the flat surface of the imbricated oblate clasts along the largest axis.

Figure 8 – Close-up photo of the lower part of Sequence 2 and upper part of Sequence 1 (and photo-interpretation). This photo shows the contact between Sequence 1 and 2 through a strike-cross section (i.e. perpendicular to the ENE to WSW palaeo-current direction; see location in Figure 7). The bottom line tracing shows most of clasts whose longest axis is at least 1 cm long (blank areas clasts are a variable mixture that covers from small pebbly sandstone to coarse-sand. The areas with the largest clasts (i.e. cobbles and large pebbles) define the downlapping bed configuration observed in Figure 7. The black arrow points to one of the interpreted bases of the amalgamated beds that make up Sequence 2. The amalgamated beds terminate as a downlap on the upper bounding surface of Sequence 1 to the NNW. Combining this downlap with that observed to the W in Figure 7, Sequence 2 appears to have had a dune-like morphology. The yellow arrow indicates the palaeocurrent direction of the CS3 canyon (i.e. ENE to WSW).

Figure 9 – Close-up of the thickest part of Sequence 3. The top photo shows the cobbly sandstone deposits with occasional boulders in the corner of Sequence 3 (where the downslope and strike cross-sections meet. Black arrows show the sharp veering of the clast imbrication azimuth from the areas with pebbly-cobbly deposits. The bottom of the figure shows a close-up of the above photo (see the white rectangle for location) with sets of imbricated cobbles with an angle of dip of 50˚ and dip direction of 280˚.

Figure 10 – Close-up of pervasive imbrication on the strike cross-section of Sequence 3. The top photo shows a general view of the clast-supported cobbly-pebbly sandstone with pervasive imbrication. The bottom photo and interpretation shows a close-up of the same deposit (see dotted rectangle for location). The photo-interpretation mostly shows the line tracing of cobbles and large pebbles with an

imbrication dip direction of 40˚/305˚ (i.e. to the NW) (the rest of pebble size also show the same imbrication). This data is This imbrication is complementary to the imbrication data included in Figure 7.

Figure 11: Stages of erosion and deposition of the Guredin palaeo-bedforms. This figure summarises the erosional and depositional processes interpreted from the sedimentary architecture of the Guredin palaeo-bedforms (for a downslope section of the CS3 canyon where they developed). This is a model suggested for the complete constructional process of these palaeo-bedforms through seven stages. 1st stage: in this particular area to the NW margin of the CS3 Canyon, low-angle cross-bedded pebbly sandstones had aggraded and produced relatively low-relief bedforms (in the range of decimetres of amplitude). 2nd stage: an erosive hydraulic jump is inferred to have developed from the chute morphology of the truncation observed for the lower bounding surface of Sequence 1, resulting in the formation of a scour. 3rd stage: the bypass of a subcritical sediment-laden flow deposited foresets of gravelly sands into the previous scour. 4th stage: deposition from gravelly sand-laden flows levelled out the previous step (the first part of the sequence showing downlapping bed configuration). 5th stage: a second erosive hydraulic jump is inferred to have developed and its roller formed a second irregular scour, probably crescent-shaped on planform view. 6th stage: a hyperconcentrated gravelly sand-laden flow (pebble to boulders), as a phase of the transformation of a major flow event, deposited part of its load into the scour created by the hydraulic jump. At this stage, the roller of the hydraulic jump either is no longer active or does not interact with the hyperconcentrated flow. The flow separation developed by the entry of the flow in the crescent-shaped scour sorts out its load (creating zones of well-defined clast-size classes, clast imbrication patterns the dune-like deposit defined by the concave-up upper bounding surface of Sequence 3). 7th stage: restoration to the deposition style of initial conditions (i.e. general low-angle cross-bed configuration with facies consisting of pebbly sandstones and traction-carpet textures).

Figure 12: Reconstruction of the complete sedimentary architecture Sequence 3. These sketches summarise the sedimentary architecture of the strike cross and downslope sections of Sequence 3 (top left and top right respectively). The grey shaded areas show three zones with different dominant clast-size classes. The part of the strike cross-section that has been reconstructed based in the morphology of an idea crescent-shaped scour, is indicated with an arrow labelled ‘Extrapolated’. The strike-cross section intends also to show the dune-like morphology that the upper bounding surface of Sequence 3

shows in Figure 7 (notice the dip directions that indicate the 3D morphology). The lower sketch shows an outline of the strike cross-section with arrows indicating the backflows interpreted from the measured imbrication patterns (notice that the central backflow direction and all of those to its right are reconstructed assuming the mirror image of the deposit).

Figure 13: Comparative analysis of streamline fields in steps. The left sketch is a redrawing of the resultant streamline field of the flume model from Allen (1968) that shows the greatest geomorphological similarity to a crescent-shaped scour. The models consists of two equally handed-step elements joined together, with downstream angle of closure of 120˚ ('reverse closure negative step') and a riser with an angle of dip of 30˚ and a constant height of ~2.5 cm. The right sketch shows a reconstruction of the possible geometrical configuration at a given moment during the deposition of Sequence 3 (particularly at the moment of the formation of the deposits exposed on the strike cross-section). The previously formed crescent-shaped scour is partially covered by the forming dune-like deposit of Sequence 3 (grey shaded area). The streamline fields on the lee-side show a backflow pattern shows the palaeocurrent directions measured in the strike-cross section of Sequence (see Figure 7). This streamline pattern is similar to that observed in the risers of Allen's model to the left. This kinematic similarity is interpreted as unequivocally indicative of a crescentic morphology for the lee-side of the dune-like deposit of Sequence 3 (implying that the same pattern is maintained during the deposition of Sequence 3 in the crescent-shaped scour). Question marks in the sketch to the right denote the uncertainty on the streamline fields on these areas.

Figure 14: Streamline field of flow separation in crescent-shaped scours. This figure shows different aspects with regard to the expected pathways of clasts based on experiments of Allen (1968). Sketch 'A' shows a planform view of the edge of a crescent-shaped scour (thick black line) with white-headed arrows indicating the lower streamline directions of the separation bubble. Rollers and vortices develop depending on the angle of attack (α) of the entering flow on the crescentic step. The threshold of the angle of attack between rollers and vortices is equal to 45˚ (labelled α'). This model has been drawn integrating results of Allen's (1968) experiments on sediment-less flow entering steps with different angles of skew, and is here proposed to be applicable to sediment-laden flows. Sketch 'B' shows a redrawing of Allen's (1968) figure of a downstream section of a separation flow (adapted to a section of a generic crescent-shaped scour). The location of this section is indicated with red marks X

and X' at the central part of the model of a crescent-shaped scour of sketch 'A'. The slope gradient value of 1.6º after and before the scour is based on real values of modern canyon slopes filled with gravelly sands (e.g. Paull et al., 2011). Sketch 'C' shows a redrawing of Allen's (1970) streamline 3D structure of rollers and vortices. A green cross and a yellow circle serve as reference points for their location at the model of sketch 'A'. Notice the closeness character of the separation bubble in a roller respect to the open one in vortices (see green line). Sketch 'D' shows a close-up of the separation bubble zone of sketch 'B' with a representation of the entrance of a generic inverse graded base of a hyperconcentrated flow. The blue, magenta and green lines show the potential clast-paths and final settling area. These paths are drawn considering as major controlling factors: the height with respect to the bottom of the lee-side and the starting velocity of the clasts (see Allen, 1968). This theoretical clast-path fit the observed zones of dominant facies types in the downslope section of Sequence 3 (see a complete reconstruction of the section of this Sequence labelled "Resultant scour-fill').

Figure 15: Constructional process of the sedimentary architecture of Sequence 3. Three stages summarise the constructional process of the second crescent-shaped scour and the dune-like deposit of Sequence 3 (green area). The figures to the left show downslope oblique views of half of the bedform evolution while those to the right show planform views. Stage 1 shows the process that formed the crescent-shaped scour by the development of a hydraulic jump on the entrance of a supercritical sediment-laden flow. Stage 2 shows the depositional process of the dune-like deposit of Sequence 3 by a subcritical sediment-laden flow with a hyperconcentrated basal structure. The stage approximately represents the moment of the deposition of the exposures where sections were logged (notice the drawing of imbricated clasts). The barchan-like dune is largely formed by the flow structure of rollers and vortices developed in the separation bubble. Stage 3 shows the final bedform. The lee-side of the resultant dune-like deposit is thought to have maintained the crescentic shape (concave downstream). However, other end morphologies are possible (see sketch to the right with the question mark). Points 'E' and 'D' are the same reference points shown in figures of the Guredin palaeo-bedform exposures.

Figure 16: Comparative analysis with bedforms of the Monterey Canyon. The top of this figure shows a bathymetrical map of the upper reach of the Monterey Canyon (modified from Figure 3 in Paull et al., 2010). The crescentic edges of the lee-side of steps are marked with a purple line. Relative bathymetric highs and lows are highlighted with red and green trace lining. Other highs and lows located

to the sides are excluded. The profile of two bathymetric sections is shown beneath the map. One follows a downslope direction, approximately crossing the central part of three crescent-shaped bedforms (A-A'). The other starts from a terrace or bench to a bathymetric high at the centre of a crescent-shaped bedform (B-B'). At the bottom, two clay models show a 3D reconstruction of the following bedforms. The first model is a reconstruction of three of the crescent-shaped bedforms of the Monterey Canyon (see the horizontal arrow on the bathymetric map). The second model is a reconstruction of the bedform resultant of the deposition of Sequence 3 in the interpreted crescent-shaped scour (equivalent to Stage 3 of Figure 15). This model shows the morphology of the resultant bedform before gravelly sands-flows deposited the low-angle cross-bedded pebbly sandstones observed overlying Sequence 3 (see the onlap terminations of Figure 5). The vertical scale is exaggerated in the clay model of the Monterey bedforms to highlight bathymetric highs and lows.

10 References

Albertson, M. L., Barton, J. R., and Simons, D. B., Fluid Mechanics for Engineers, Prentice-Hall, Englewood Cliffs, NY, 1960.

Allen, J.R.L., 1965. Sedimentation to the lee of small underwater sand waves: an experimental study. The Journal of Geology, 73(1), pp.95-116.

Allen, J.R.L., 1968. Current Ripples. North-Holland, 433 pp.

Allen J. R. L.1970. Physical Processes of Sedimentation. xv + 248 pp., figs. George Allen and Unwin Ltd., London.

Allen, J.R.L., 1982. Sedimentary structures, their character and physical basis (Vol. 1). Elsevier.

Allen, J.R.L., 1983. Studies in fluviatile sedimentation: bars, bar-complexes and sandstone sheets (low-sinuosity braided streams) in the Brownstones (L. Devonian), Welsh Borders. Sedimentary Geology, 33(4), pp.237-293.

1167 Arzola, R.G., Wynn, R.B., Lastras, G., Masson, D.G. and Weaver, P.P., 2008. Sedimentary features
1168 and processes in the Nazaré and Setúbal submarine canyons, west Iberian margin. Marine Geology,
1169 250(1), pp.64-88.

1170 Azpiroz-Zabala, M., Cartigny, M.J., Talling, P.J., Parsons, D.R., Sumner, E.J., Clare, M.A., Simmons,
1171 S.M., Cooper, C. and Pope, E.L., 2017. Newly recognized turbidity current structure can explain
1172 prolonged flushing of submarine canyons. Science advances, *3*(10), p.e1700200.

1173 Bagnold, R.A., 1954, August. Experiments on a gravity-free dispersion of large solid spheres in a
1174 Newtonian fluid under shear. In Proceedings of the Royal Society of London A: Mathematical, Physical
1175 and Engineering Sciences (Vol. 225, No. 1160, pp. 49-63). The Royal Society.

1176 Bouma, A.H. and Treadwell, T.K., 1975. Deep-sea dune-like features. Marine Geology, 19(5), pp.M53-
1177 M59.

1178 Carling, P.A., 1999. Subaqueous gravel dunes. Journal of Sedimentary Research, 69(3).

1179 Cartigny, M.J., Postma, G., van den Berg, J.H. and Mastbergen, D.R., 2011. A comparative study of
1180 sediment waves and cyclic steps based on geometries, internal structures and numerical modeling.
1181 Marine Geology, 280(1), pp.40-56.

1182 Cartigny, M.J., Ventra, D., Postma, G. and Den Berg, J.H., 2014. Morphodynamics and sedimentary
1183 structures of bedforms under supercritical-flow conditions: New insights from flume experiments.
1184 Sedimentology, 61(3), pp.712-748.

1185 Chanson, H., 2004. The Hydraulics of Open Channel Flows: An Introduction. Butterworth-Heinemann,
1186 Oxford, UK, 2nd edition, 630 pp.

1187 Coordinated Canyon Experiment, 2017, December 11. Retrieved from https://www.mbari.org/multi-year-
1188 submarine-canyon-study-challenges-textbook-theories-about-turbidity-currents/.

1189 Cronin, B. T., Gürbüz, K., Gül, M., Çelik, H., Hurst, A. and Kelling, G., 2008. Evolution of multiphase,
1190 winged, coarse-grained deep-water canyons: the Alikayası Canyon, Miocene, eastern Turkey. Atlas of
1191 Deep-Water Outcrops: AAPG Memoir, Studies in Geology, 56, pp.357-362.

1192 Duarte, J.C., Terrinha, P., Rosas, F.M., Valadares, V., Pinheiro, L.M., Matias, L., Magalhães, V. and
1193 Roque, C., 2010. Crescent-shaped morphotectonic features in the Gulf of Cadiz (offshore SW Iberia).
1194 Marine Geology, 271(3-4), pp.236-249.

1195 Hughes Clarke, J.E., 2016. First wide-angle view of channelized turbidity currents links migrating cyclic
1196 steps to flow characteristics. Nature communications, 7, p.11896.

1197 Ito, M. and Saito, T., 2006. Gravel waves in an ancient canyon: analogous features and formative
1198 processes of coarse-grained bedforms in a submarine-fan system, the Lower Pleistocene of the Boso
1199 Peninsula, Japan. Journal of Sedimentary Research, 76(12), pp.1274-1283.

1200 Fildani, A., Normark, W.R., Kostic, S. and Parker, G., 2006. Channel formation by flow stripping: Large-
1201 scale scour features along the Monterey East Channel and their relation to sediment waves.
1202 Sedimentology, 53(6), pp.1265-1287.

1203 Friend, P.F., Slater, M.J. and Williams, R.C., 1979. Vertical and lateral building of river sandstone
1204 bodies, Ebro Basin, Spain; J. Geol. Soc. London, y. 136, p. 39-46.

1205 Galvin, C., 2003. Imbrication and flow-oriented clasts. Middleton, GV (ed.) Encyclopedia of Sediments
1206 and Sedimentary Rocks: 371-374.

1207 Gorard, S., 2005. Revisiting a 90-year-old debate: the advantages of the mean deviation. British Journal
1208 of Educational Studies, 53(4), pp.417-430.

1209 Gül, M., Gürbüz, K. and Cronin, B.T., 2011. Provenance of the northern part of the Kahramanmaraş
1210 peripheral foreland basin (Miocene, S Turkey). Journal of Asian Earth Sciences, 40(2), pp.475-495.

1211 Gül, M., Cronin, B.T. and Gürbüz, K., 2012. Confined deep water system development on the
1212 accretionary wedge (Miocene, Kahramanmaraş Foreland Basin, S Turkey). Earth-science reviews,
1213 114(3), pp.195-217.

1214 Hüsing, S. K., Zachariasse, W. J., Van Hinsbergen, D. J., Krijgsman, W., Inceöz, M., Harzhauser, M.,
1215 Mandic, O. and Kroh, A., 2009. Oligocene–Miocene basin evolution in SE Anatolia, Turkey: constraints
1216 on the closure of the eastern Tethys gateway. Geological Society, London, Special Publications, 311(1),
1217 pp.107-132.

1218 Jopling, A.V., 1964. Laboratory study of sorting processes related to flow separation. Journal of
1219 Geophysical Research, 69(16), pp.3403-3418.

1220 Jopling, A.V., 1965. Hydraulic factors controlling the shape of laminae in laboratory deltas. J. Sediment.
1221 Petrol., 35, 777-791

1222 Kneller, B., 1995. Beyond the turbidite paradigm: physical models for deposition of turbidites and their
1223 implications for reservoir prediction. Geological Society, London, Special Publications, 94(1), pp.31-49.

1224 Kostic, S., 2011. Modeling of submarine cyclic steps: Controls on their formation, migration, and
1225 architecture. Geosphere, 7(2), pp.294-304.

1226 Kostic, S. and Parker, G., 2006. The response of turbidity currents to a canyon–fan transition: internal
1227 hydraulic jumps and depositional signatures. Journal of Hydraulic Research, 44(5), pp.631-653.

1228 Kostic, S., Sequeiros, O., Spinewine, B. and Parker, G., 2010. Cyclic steps: A phenomenon of
1229 supercritical shallow flow from the high mountains to the bottom of the ocean. Journal of Hydro-
1230 environment Research, 3(4), pp.167-172.

1231 Lamb, M.P., Parsons, J.D., Mullenbach, B.L., Finlayson, D.P., Orange, D.L. and Nittrouer, C.A., 2008.
1232 Evidence for superelevation, channel incision, and formation of cyclic steps by turbidity currents in Eel
1233 Canyon, California. Geological Society of America Bulletin, 120(3-4), pp.463-475.

1234 Lewis, K.B. and Pantin, H.M., 2002. Channel-axis, overbank and drift sediment waves in the southern
1235 Hikurangi Trough, New Zealand. Marine Geology, 192(1), pp.123-151.

1236 Lopez Jimenez, R., 2017. Sedimentary architecture of ancient submarine channel systems of the Maraş
1237 Basin (Kahramanmaraş Province, Turkey). PhD Thesis. University of Aberdeen.

1238 Lopez Jimenez, R., Cronin, B.T., Turner, C.C., Çelik, H., Bastidas, R. and Kneller, B.C., 2018. The
1239 Alikayası Canyon-Channel System (Miocene, SE Turkey) compared with the South Brae Fan System
1240 (Upper Jurassic, North Sea); Characterising sand and gravel filled channel complexes in coarse-grained
1241 deep-water systems without gravel cone geometries. in Colin C. Turner and Bryan T. Cronin, ed, Rift-
1242 related coarse-grained submarine fan reservoirs; the Brae Play, South Viking Graben, North Sea:
1243 Memoir 115.

1244 Malinverno, A., Ryan, W.B., Auffret, G. and Pautot, G., 1988. Sonar images of the path of recent failure
1245 events on the continental margin off Nice, France. Geological Society of America Special Papers, 229,
1246 pp.59-76.

1247 Miall, A.D., 1985. Architectural-element analysis: a new method of facies analysis applied to fluvial
1248 deposits. Earth-Sci. Rev., 22: 261-308.

1249 Middleton, G.V., 1970. Experimental studies related to problems of flysch sedimentation, in Lajoie, J.,
1250 ed., Flysch Sedimentology in North America: Geol. Assoc. Canada Spec. Paper 7, pp. 253-272.

1251 Middleton, G.V. and Hampton, M.A., 1973. Part I. Sediment gravity flows: mechanics of flow and
1252 deposition, in G. V. Middleton and A. H. Bouma (eds.), Turbidites and Deep Water Sedimentation.
1253 Anaheim, California, S.E.P.M. Pacific Section Short Course Notes, pp 1-38.

1254 Migeon, S., Savoye, B., Zanella, E., Mulder, T., Faugères, J.C. and Weber, O., 2001. Detailed seismic-
1255 reflection and sedimentary study of turbidite sediment waves on the Var Sedimentary Ridge (SE
1256 France): significance for sediment transport and deposition and for the mechanisms of sediment-wave
1257 construction. Marine and Petroleum Geology, 18(2), pp.179-208.

1258 Mitchell, N.C., 2006. Morphologies of knickpoints in submarine canyons. Geological Society of America
1259 Bulletin, 118(5-6), pp.589-605.

1260 Mulder, T. and Alexander, J., 2001. The physical character of subaqueous sedimentary density flows
1261 and their deposits. Sedimentology, 48(2), pp.269-299.

1262 Mutti, E. and Normark, W.R., 1987. Comparing examples of modern and ancient turbidite systems:
1263 problems and concepts. In Marine clastic sedimentology (pp. 1-38). Springer Netherlands.

1264 Normandeau, A., Lajeunesse, P., St-Onge, G., Bourgault, D., Drouin, S.S.O., Senneville, S. and
1265 Bélanger, S., 2014. Morphodynamics in sediment-starved inner-shelf submarine canyons (Lower St.
1266 Lawrence Estuary, Eastern Canada). Marine Geology, 357, pp.243-255.

1267 Normark, W.R., Hess, G.R., Stow, D.A.V. and Bowen, A.J., 1980. Sediment waves on the Monterey Fan
1268 levee: a preliminary physical interpretation. Marine Geology, 37(1-2), pp.1-18.

1269 Normark, W. R., Piper, D. J. W., 1991, Initiation processes and flow evolution of turbidity currents:
1270 Implications for the depositional record. In: Osborn, R. H. (Ed.), From Shoreline to Abyss:
1271 Contributions in Marine Geology in Honor of Francis Parker Shepard, Tulsa, OK, Society of
1272 Economic Paleontologists and Mineralogists Special Publication No. 46, pp. 207-230.

1273 Önalan, M., 1986. K. Maraş tersiyer istifinin sedimenter özellikleri ve çökelme ortamlari. İstanbul
1274 Yerbilimleri Dergisi, 5(1-2), pp.39-78.

1275 Parker, G. and Izumi, N., 2000. Purely erosional cyclic and solitary steps created by flow over a
1276 cohesive bed. Journal of Fluid Mechanics, 419, pp.203-238.

1277 Paull, C.K., Ussler III, W., Caress, D.W., Lundsten, E., Covault, J.A., Maier, K.L., Xu, J. and Augenstein,
1278 S., 2010. Origins of large crescent-shaped bedforms within the axial channel of Monterey Canyon,
1279 offshore California. Geology, 6(6), pp.755-774.

1280 Paull, C.K., Caress, D.W., Ussler, W., Lundsten, E. and Meiner-Johnson, M., 2011. High-resolution
1281 bathymetry of the axial channels within Monterey and Soquel submarine canyons, offshore central
1282 California. Geosphere, 7(5), pp.1077-1101.

1283 Piper, D.J. and Savoye, B., 1993. Processes of late Quaternary turbidity current flow and deposition on
1284 the Var deep-sea fan, north-west Mediterranean Sea. Sedimentology, 40(3), pp.557-582.

1285 Piper, D.J., Shor, A.N., Farre, J.A., O'Connell, S. and Jacobi, R., 1985. Sediment slides and turbidity
1286 currents on the Laurentian Fan: Sidescan sonar investigations near the epicenter of the 1929 Grand
1287 Banks earthquake. Geology, 13(8), pp.538-541.

1288 Piper, D.J. and Kontopoulos, N., 1994. Bed forms in submarine channels: comparison of ancient
1289 examples from Greece with studies of Recent turbidite systems. Journal of Sedimentary Research,
1290 64(2).

1291 Postma, G., Nemec, W. and Kleinspehn, K.L., 1988. Large floating clasts in turbidites: a mechanism for
1292 their emplacement. Sedimentary geology, 58(1), pp.47-61.

1293 Postma, G., Cartigny, M. and Kleverlaan, K., 2009. Structureless, coarse-tail graded Bouma Ta formed
1294 by internal hydraulic jump of the turbidity current?. Sedimentary Geology, 219(1), pp.1-6.

1295 Postma, G., Kleverlaan, K. and Cartigny, M.J., 2014. Recognition of cyclic steps in sandy and gravelly
1296 turbidite sequences, and consequences for the Bouma facies model. Sedimentology, 61(7), pp.2268-
1297 2290.

1298 Shor, A.N., Piper, D.J., Clarke, J.E.H. and Mayer, L.A., 1990. Giant flute-like scour and other erosional
1299 features formed by the 1929 Grand Banks turbidity current. Sedimentology, 37(4), pp.631-645.

1300 Smith, D.P., Ruiz, G., Kvitek, R. and Iampietro, P.J., 2005. Semiannual patterns of erosion and
1301 deposition in upper Monterey Canyon from serial multibeam bathymetry. Geological Society of America
1302 Bulletin, 117(9-10), pp.1123-1133.

1303 Smith, D.P., Kvitek, R., Iampietro, P.J. and Wong, K., 2007. Twenty-nine months of geomorphic change
1304 in upper Monterey Canyon (2002–2005). Marine Geology, 236(1), pp.79-94.

1305 Sohn, Y.K., 1997. On traction carpet sedimentation. Journal of Sedimentary Research, 67(3).

1306 Sumner, E.J. and Paull, C.K., 2014. Swept away by a turbidity current in Mendocino submarine canyon,
1307 California. Geophysical Research Letters, 41(21), pp.7611-7618.

1308 Symons, W.O., Sumner, E.J., Talling, P.J., Cartigny, M.J. and Clare, M.A., 2016. Large-scale sediment
1309 waves and scours on the modern seafloor and their implications for the prevalence of supercritical
1310 flows. Marine Geology, 371, pp.130-148.

1311 Symons, W.O., Sumner, E.J., Paull, C.K., Cartigny, M.J., Xu, J.P., Maier, K.L., Lorenson, T.D. and
1312 Talling, P.J., 2017. A new model for turbidity current behavior based on integration of flow monitoring
1313 and precision coring in a submarine canyon. *Geology*, *45*(4), pp.367-370.

1314 Taki, K. and Parker, G., 2005. Transportational cyclic steps created by flow over an erodible bed. Part 1.
1315 Experiments. Journal of Hydraulic Research, 43(5), pp.488-501.

1316 Tubau, X., Canals, M., Lastras, G., Rayo, X., Rivera, J. and Amblas, D., 2015. Marine litter on the floor
1317 of deep submarine canyons of the Northwestern Mediterranean Sea: the role of hydrodynamic
1318 processes. Progress in Oceanography, 134, pp.379-403.

Walker, R.G., 1965, June. The origin and significance of the internal sedimentary structures of turbidites. In Proceedings of the Yorkshire Geological and Polytechnic Society (Vol. 35, No. 1, pp. 1-32). Geological Society of London.

Winn, R.D. and Dott, R.H., 1977. Large-scale traction-produced structures in deep-water fan-channel conglomerates in southern Chile. Geology, 5(1), pp.41-44.

Wynn, R.B., Masson, D.G., Stow, D.A. and Weaver, P.P., 2000. Turbidity current sediment waves on the submarine slopes of the western Canary Islands. Marine Geology, 163(1), pp.185-198.

Wynn, R.B. and Stow, D.A., 2002. Classification and characterisation of deep-water sediment waves. Marine Geology, 192(1), pp.7-22.

Zhong, G., Cartigny, M.J., Kuang, Z. and Wang, L., 2015. Cyclic steps along the South Taiwan Shoal and West Penghu submarine canyons on the northeastern continental slope of the South China Sea. Geological Society of America Bulletin, 127(5-6), pp.804-824.

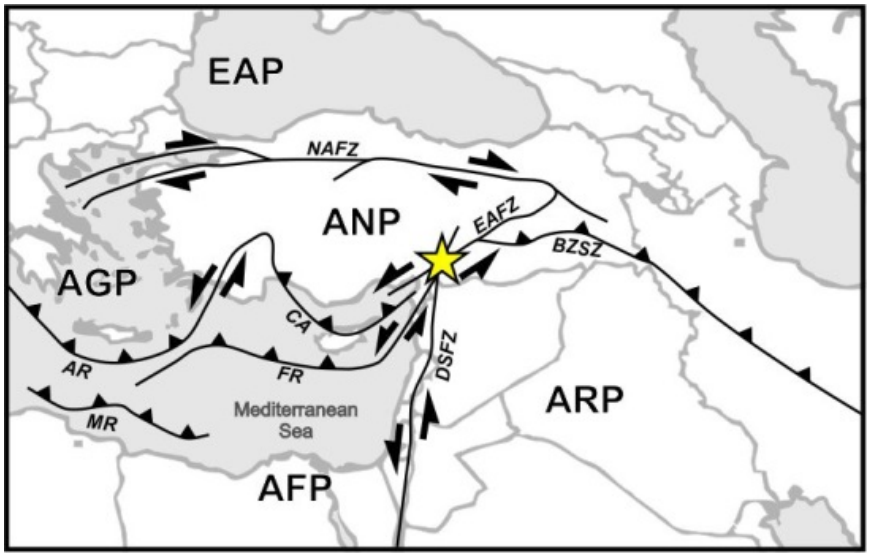

Figure 1

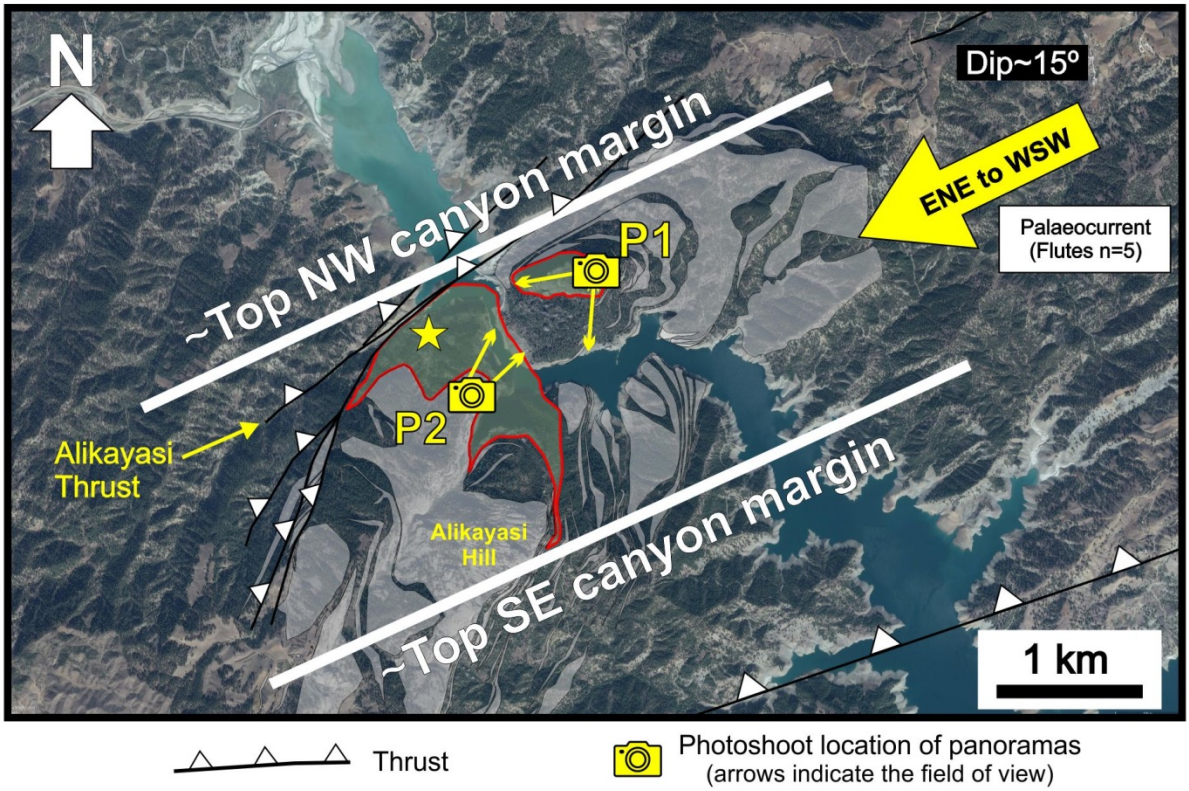

Figure 2

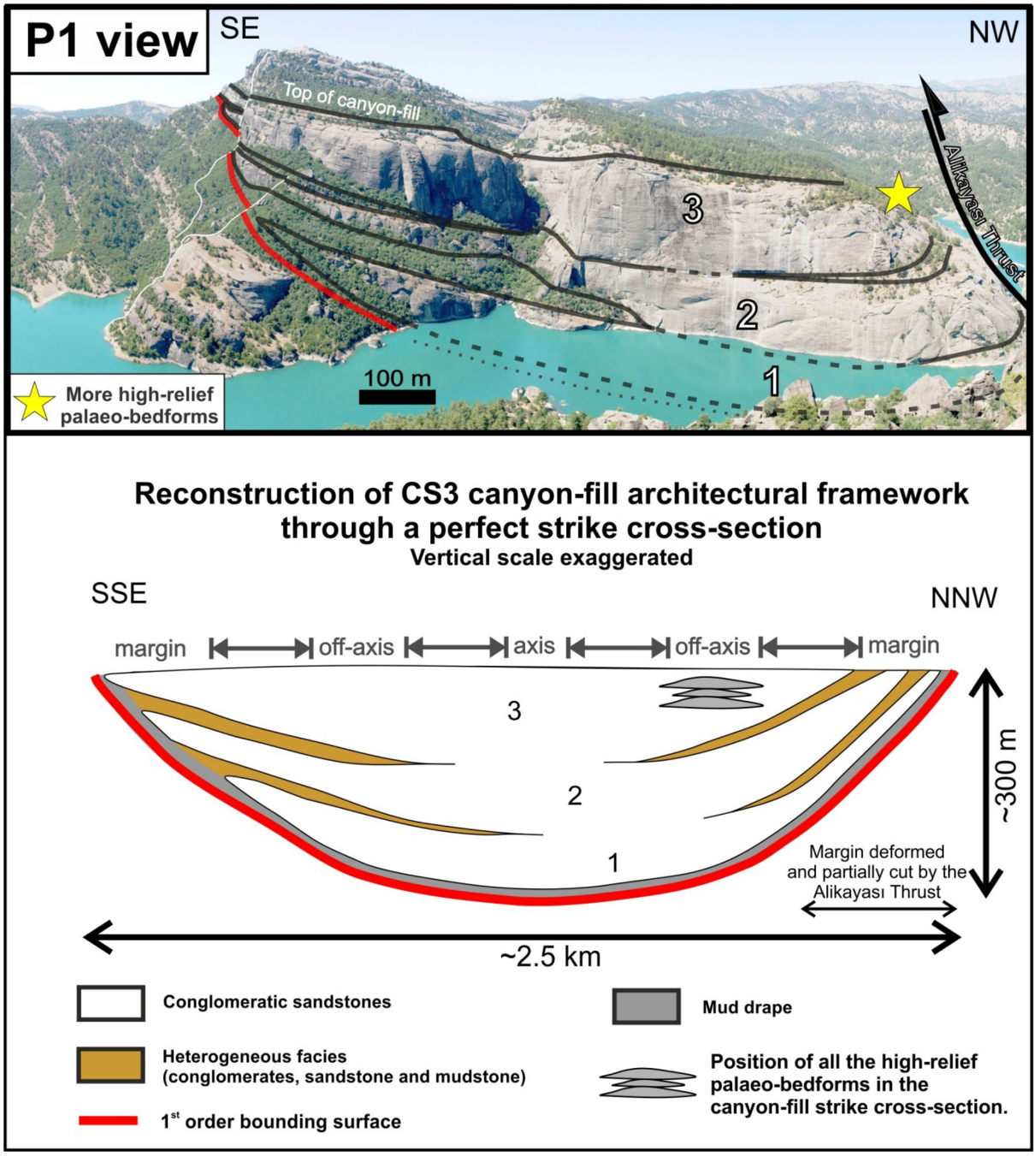
P1 view
SE
NW
Top of canyon-fill
Alikayası Thrust
3
2
1
100 m
More high-relief palaeo-bedforms
Reconstruction of CS3 canyon-fill architectural framework through a perfect strike cross-section
Vertical scale exaggerated
SSE
NNW
margin
off-axis
axis
off-axis
margin
3
2
1
~300 m
Margin deformed and partially cut by the Alikayası Thrust
~2.5 km
Conglomeratic sandstones
Mud drape
Heterogeneous facies (conglomerates, sandstone and mudstone)
Position of all the high-relief palaeo-bedforms in the canyon-fill strike cross-section.
1st order bounding surface

Figure 3

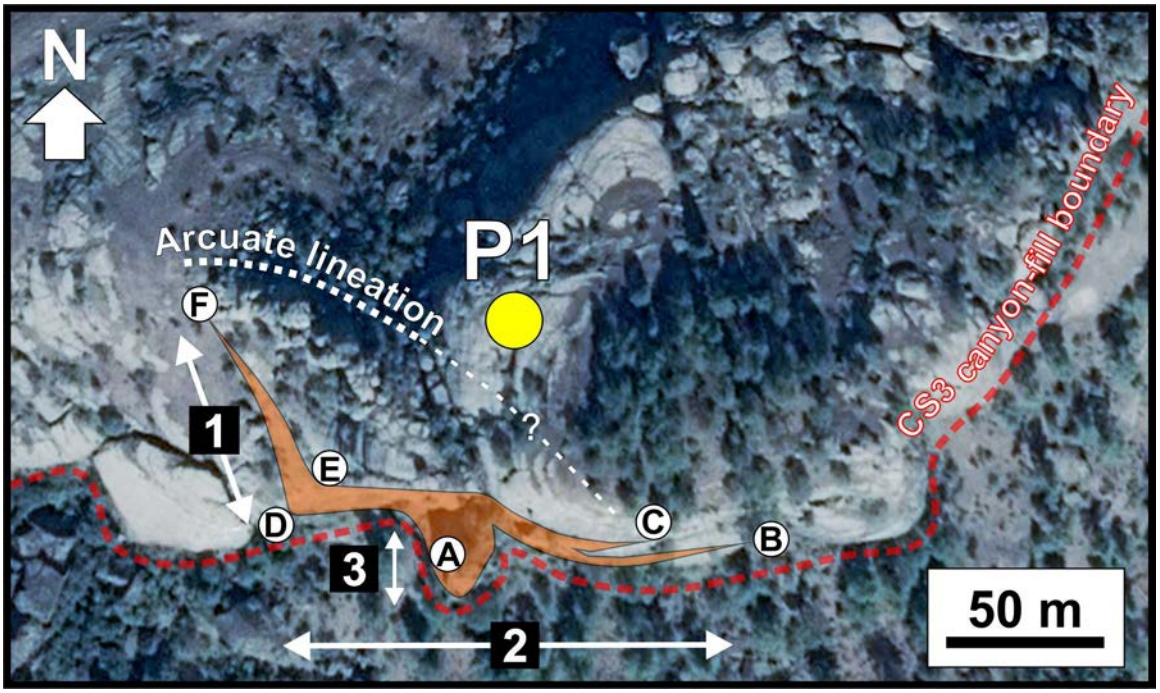
N
Arcuate lineation
P1
F
1
E
D
3
A
C
B
2
CS3 canyon-fill boundary
50 m

Figure 4

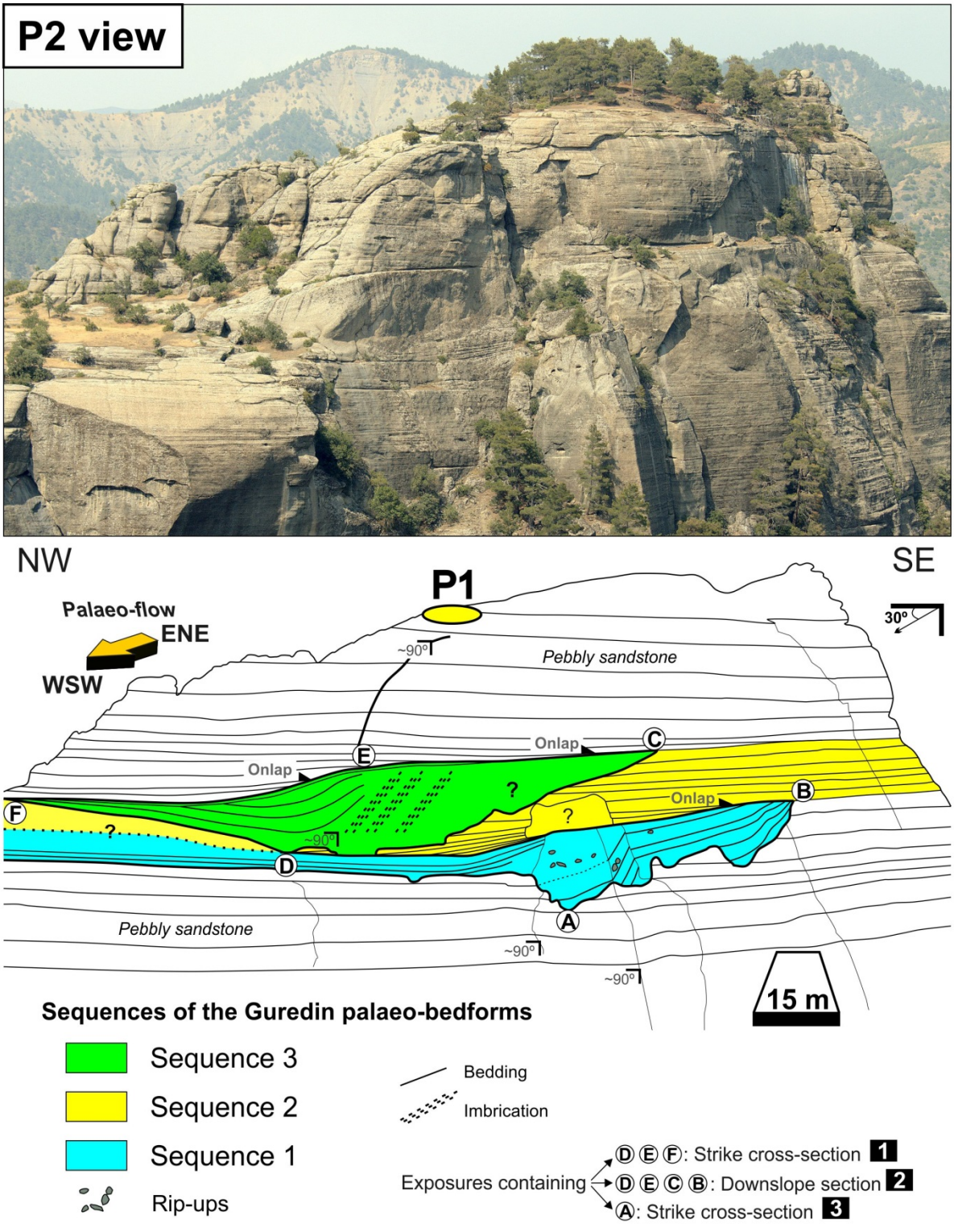
P2 view
NW
SE
P1
Palaeo-flow
ENE
WSW
~90°
Pebbly sandstone
30°
Onlap
Onlap
Onlap
C
E
B
F
D
A
?
?
?
~90°
Pebbly sandstone
~90°
~90°
15 m
Sequences of the Guredin palaeo-bedforms
Sequence 3
Sequence 2
Sequence 1
Rip-ups
Bedding
Imbrication
Exposures containing
Ⓓ Ⓔ Ⓕ: Strike cross-section 1
Ⓓ Ⓔ Ⓒ Ⓑ: Downslope section 2
Ⓐ: Strike cross-section 3

Figure 5

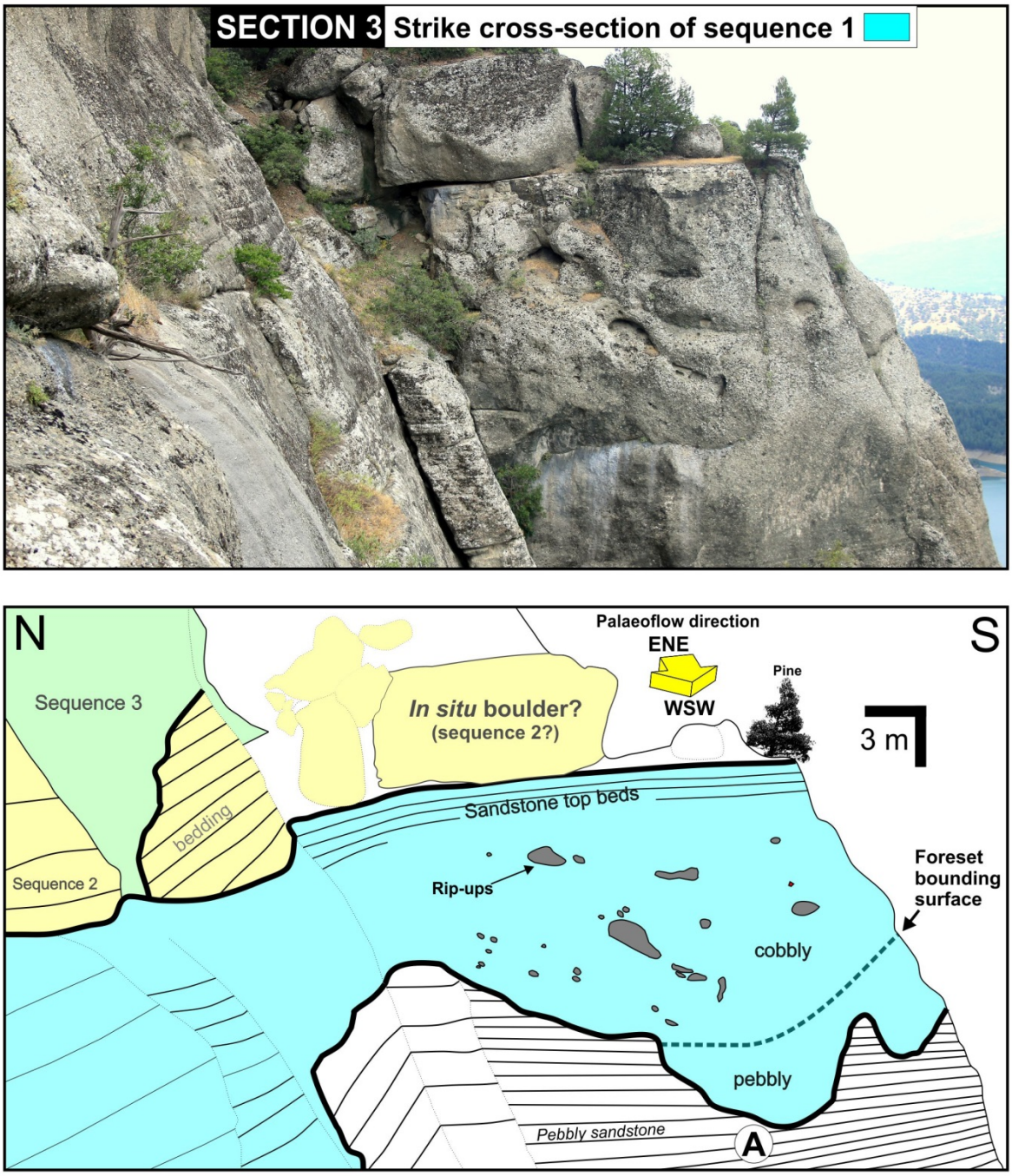
SECTION 3 Strike cross-section of sequence 1
N
S
Palaeoflow direction
ENE
WSW
Pine
3 m
Sequence 3
Sequence 2
bedding
In situ boulder?
(sequence 2?)
Sandstone top beds
Rip-ups
Foreset bounding surface
cobbly
pebbly
Pebbly sandstone
A

Figure 6

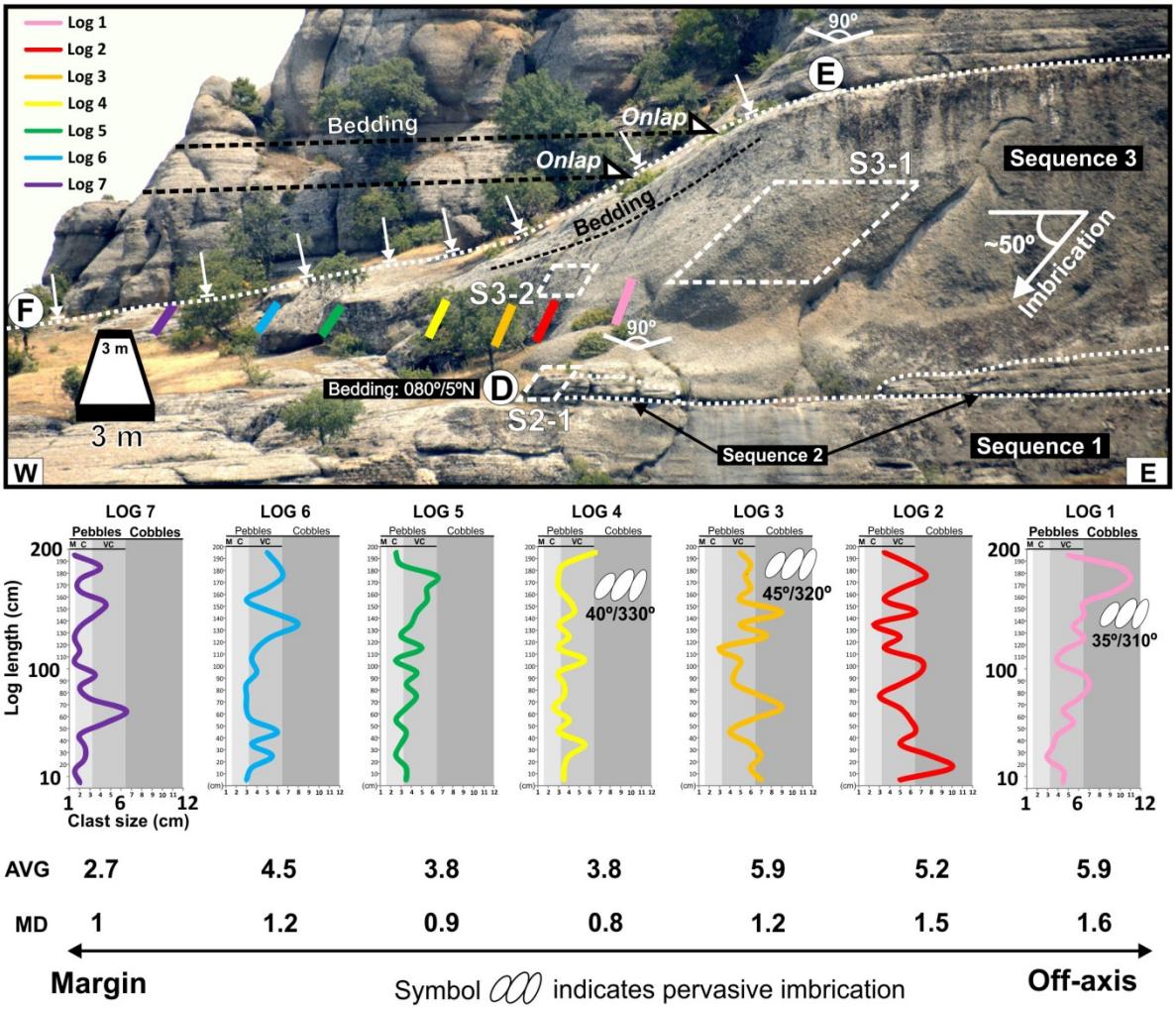
Log 1
Log 2
Log 3
Log 4
Log 5
Log 6
Log 7
Bedding
Onlap
Onlap
Bedding
S3-1
Sequence 3
S3-2
S2-1
Sequence 2
Sequence 1
90°
90°
E
F
D
~50°
Imbrication
3 m
3 m
Bedding: 080°/5°N
W
E
LOG 7
LOG 6
LOG 5
LOG 4
LOG 3
LOG 2
LOG 1
Pebbles Cobbles
M C VC
Log length (cm)
200
100
10
1
6
12
Clast size (cm)
40°/330°
45°/320°
35°/310°
AVG 2.7 4.5 3.8 3.8 5.9 5.2 5.9
MD 1 1.2 0.9 0.8 1.2 1.5 1.6
Margin
Symbol indicates pervasive imbrication
Off-axis

Figure 7

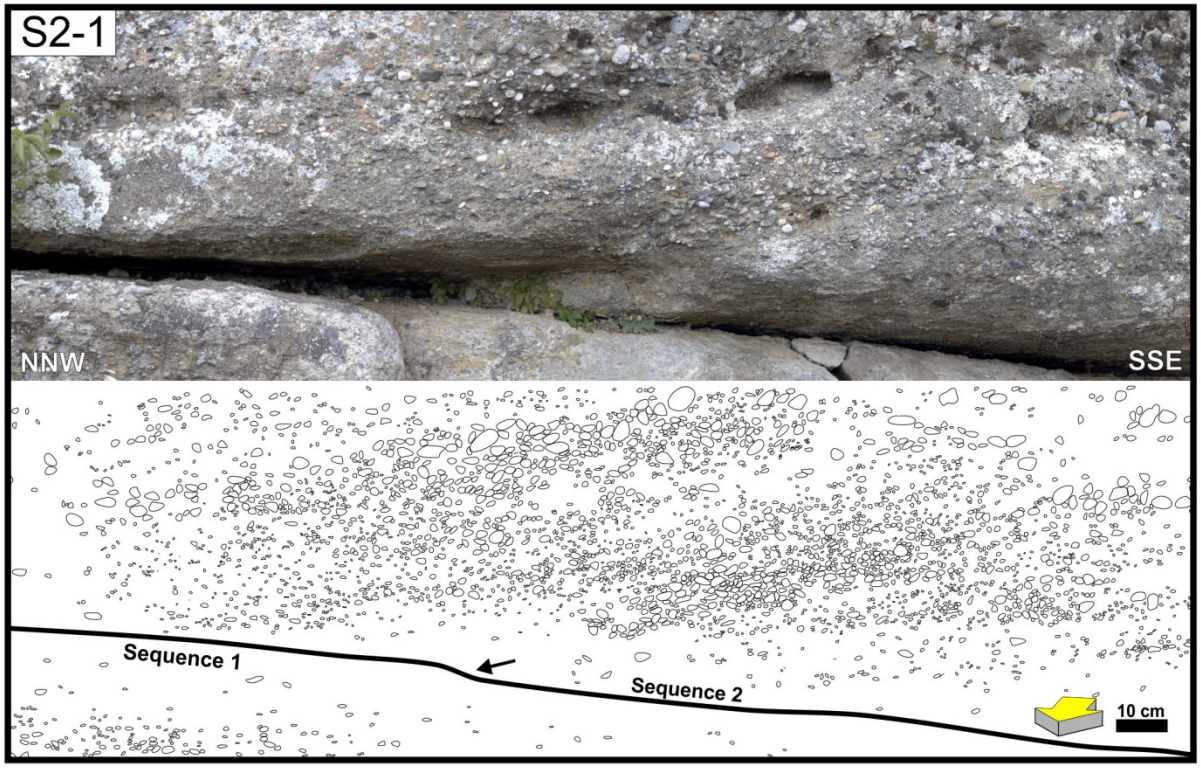

Figure 8

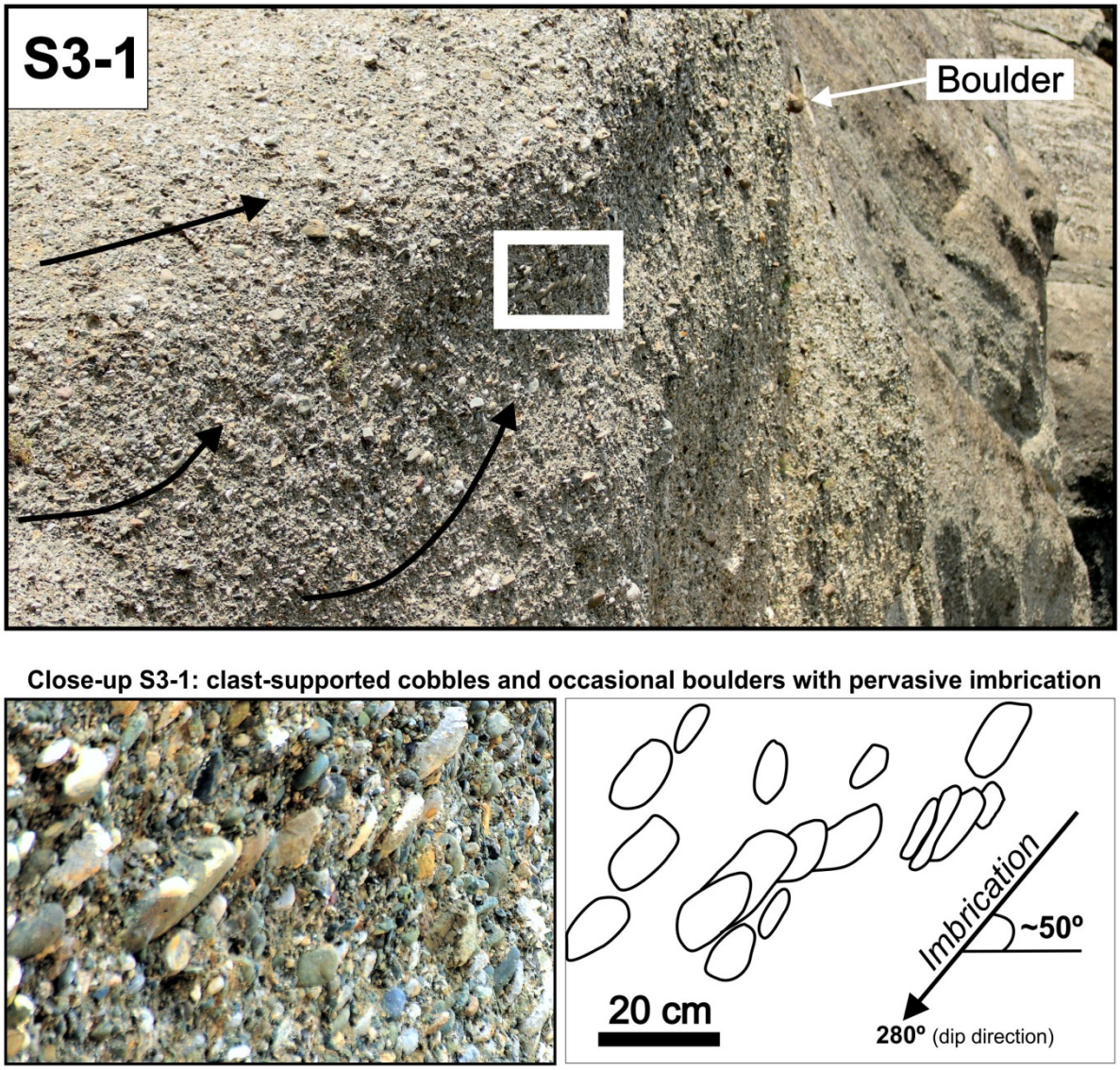
S3-1
Boulder
Close-up S3-1: clast-supported cobbles and occasional boulders with pervasive imbrication
Imbrication
~50°
20 cm
280° (dip direction)

Figure 9

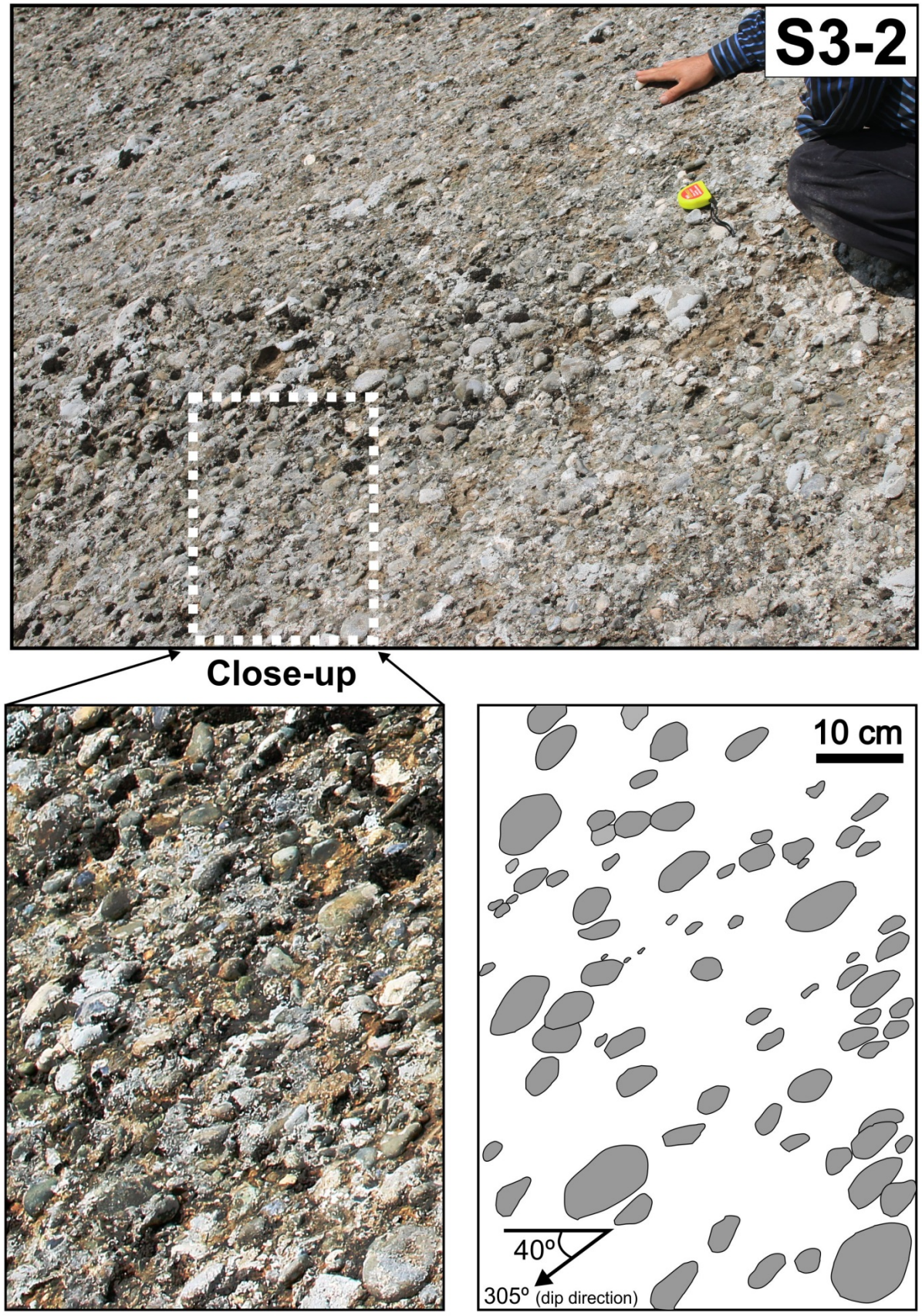

Figure 10

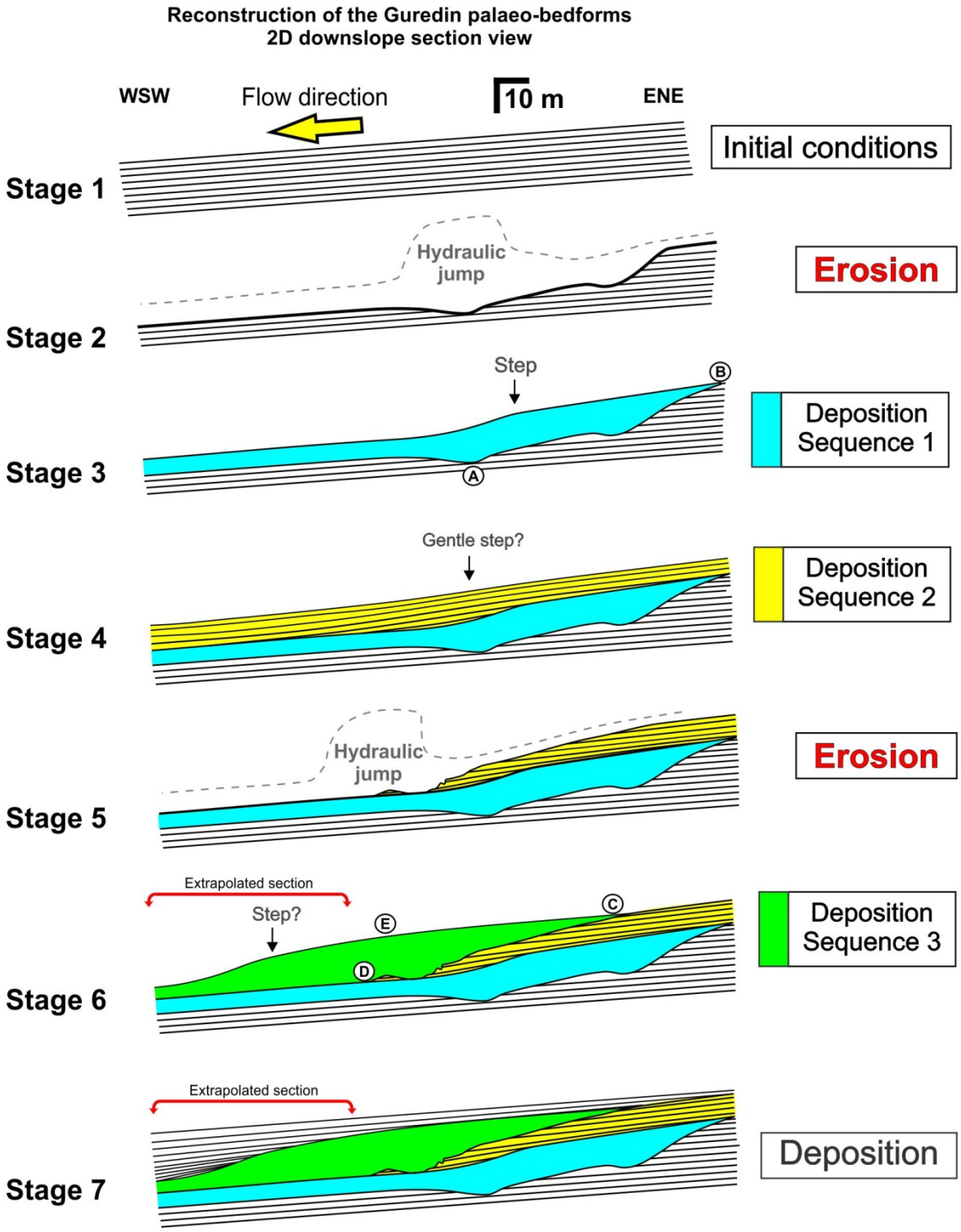
Reconstruction of the Guredin palaeo-bedforms
2D downslope section view
WSW
Flow direction
10 m
ENE
Stage 1
Initial conditions
Hydraulic jump
Erosion
Stage 2
Step
B
A
Stage 3
Deposition Sequence 1
Gentle step?
Stage 4
Deposition Sequence 2
Hydraulic jump
Erosion
Stage 5
Extrapolated section
Step?
E
C
D
Stage 6
Deposition Sequence 3
Extrapolated section
Stage 7
Deposition

Figure 11

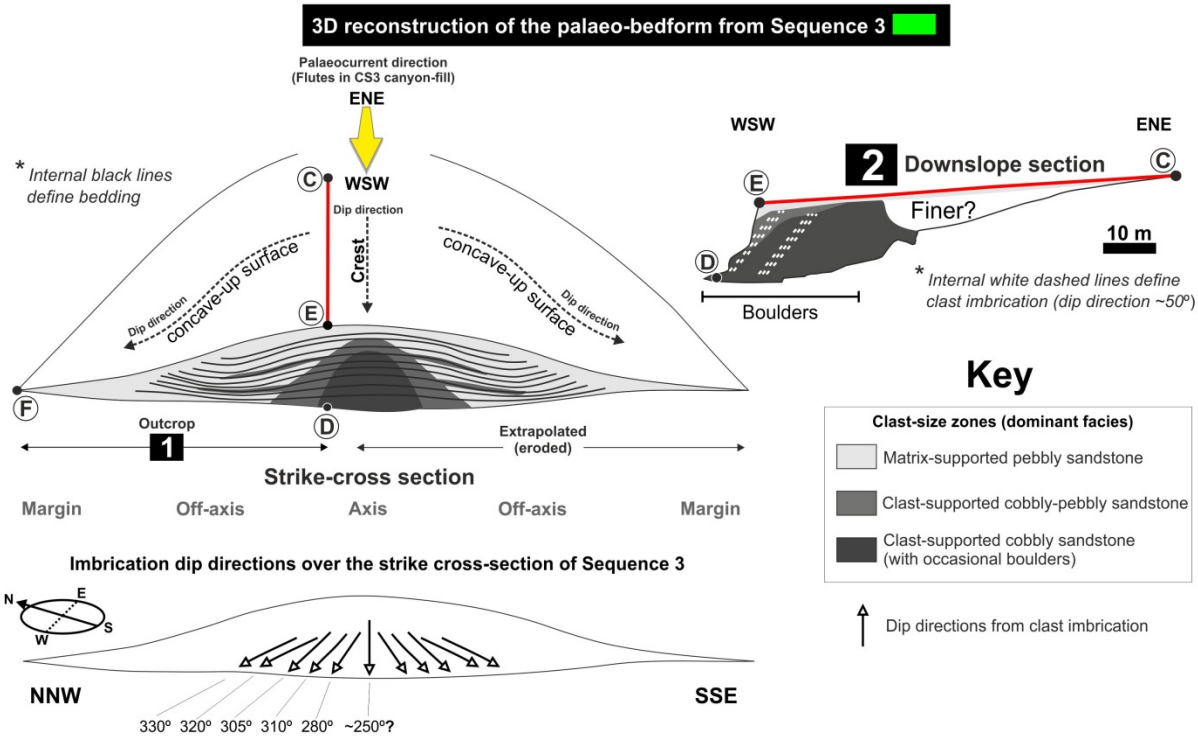
3D reconstruction of the palaeo-bedform from Sequence 3
Palaeocurrent direction
(Flutes in CS3 canyon-fill)
ENE
* Internal black lines define bedding
C
WSW
Dip direction
Crest
concave-up surface
Dip direction
concave-up surface
Dip direction
E
F
Outcrop
1
D
Extrapolated
(eroded)
Strike-cross section
Margin
Off-axis
Axis
Off-axis
Margin
WSW
ENE
2 Downslope section
C
E
Finer?
10 m
D
Boulders
* Internal white dashed lines define clast imbrication (dip direction ~50º)
Key
Clast-size zones (dominant facies)
Matrix-supported pebbly sandstone
Clast-supported cobbly-pebbly sandstone
Clast-supported cobbly sandstone (with occasional boulders)
Dip directions from clast imbrication
Imbrication dip directions over the strike cross-section of Sequence 3
N
E
S
W
NNW
SSE
330º 320º 305º 310º 280º ~250º?

Figure 12

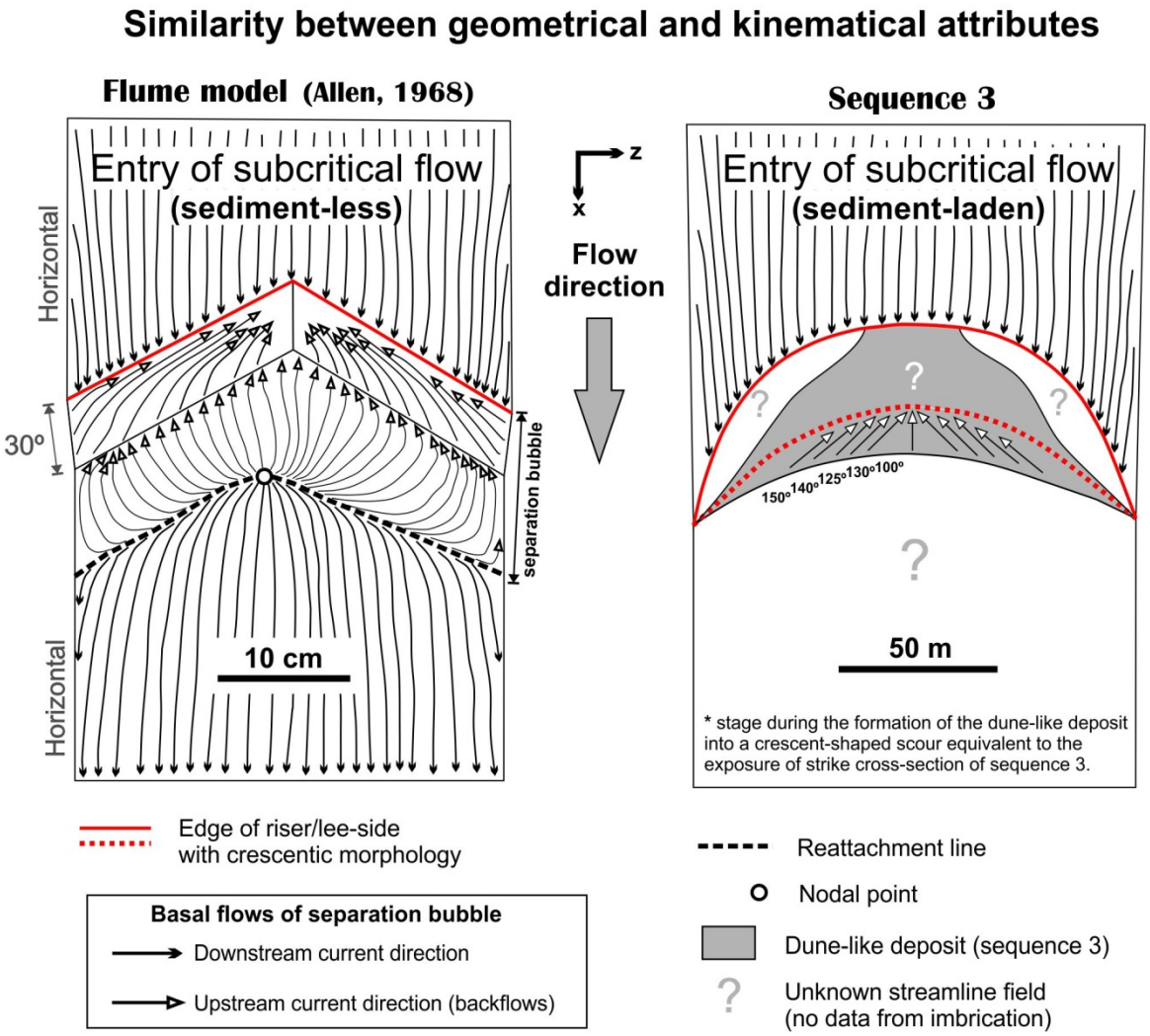
Similarity between geometrical and kinematical attributes
Flume model (Allen, 1968)
Entry of subcritical flow
(sediment-less)
Horizontal
30°
separation bubble
10 cm
Horizontal
z
x
Flow direction
Sequence 3
Entry of subcritical flow
(sediment-laden)
?
?
?
150°140°125°130°100°
?
50 m
* stage during the formation of the dune-like deposit into a crescent-shaped scour equivalent to the exposure of strike cross-section of sequence 3.
Edge of riser/lee-side with crescentic morphology
Basal flows of separation bubble
Downstream current direction
Upstream current direction (backflows)
Reattachment line
Nodal point
Dune-like deposit (sequence 3)
Unknown streamline field (no data from imbrication)

Figure 13

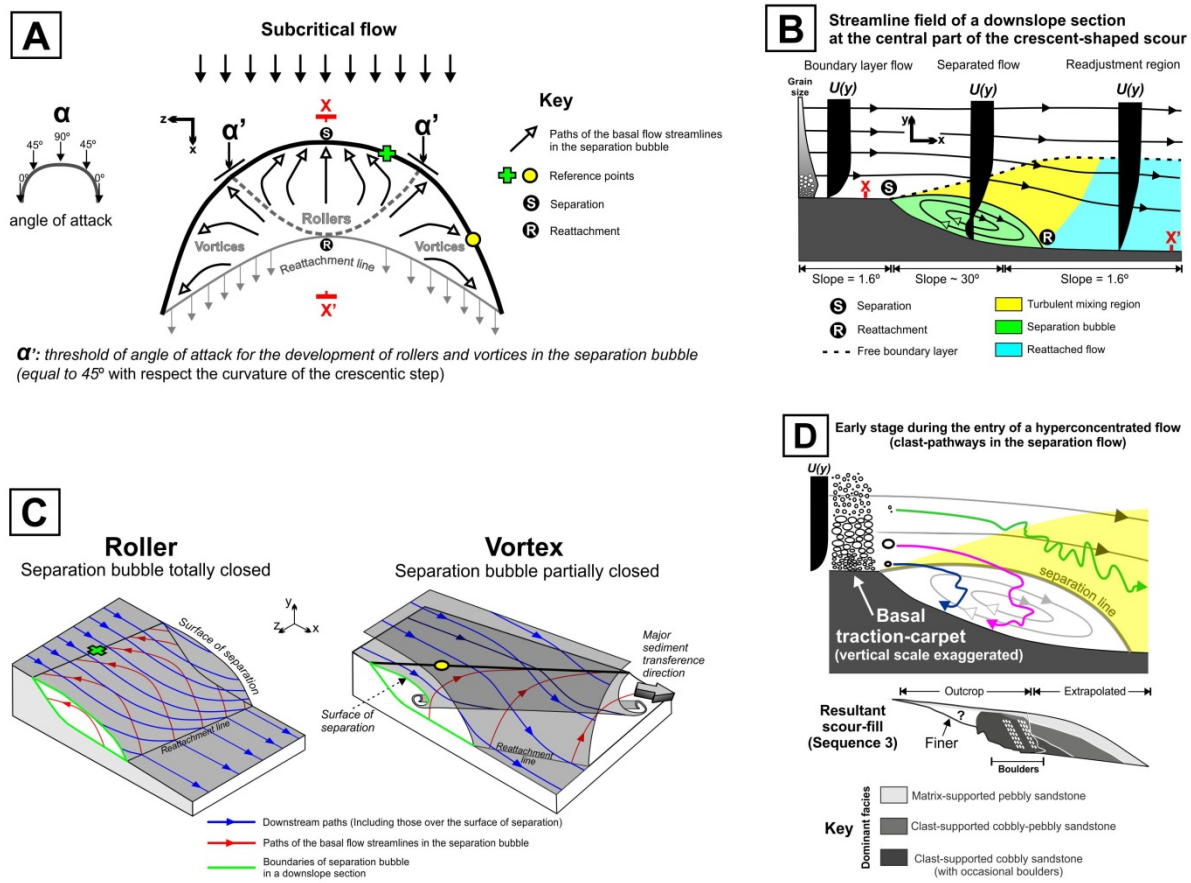
A
Subcritical flow
α
45°
90°
45°
0°
0°
angle of attack
α'
α'
Rollers
Vortices
Vortices
Reattachment line
Key
Paths of the basal flow streamlines in the separation bubble
Reference points
Separation
Reattachment
α': threshold of angle of attack for the development of rollers and vortices in the separation bubble (equal to 45º with respect the curvature of the crescentic step)
B
Streamline field of a downslope section at the central part of the crescent-shaped scour
Boundary layer flow
Separated flow
Readjustment region
Grain size
U(y)
U(y)
U(y)
Slope = 1.6°
Slope ~ 30°
Slope = 1.6°
Separation
Reattachment
Free boundary layer
Turbulent mixing region
Separation bubble
Reattached flow
C
Roller
Separation bubble totally closed
Vortex
Separation bubble partially closed
Surface of separation
Reattachment line
Surface of separation
Major sediment transference direction
Reattachment line
Downstream paths (Including those over the surface of separation)
Paths of the basal flow streamlines in the separation bubble
Boundaries of separation bubble in a downslope section
D
Early stage during the entry of a hyperconcentrated flow (clast-pathways in the separation flow)
U(y)
separation line
Basal traction-carpet (vertical scale exaggerated)
Outcrop
Extrapolated
Resultant scour-fill (Sequence 3)
Finer
Boulders
Key
Dominant facies
Matrix-supported pebbly sandstone
Clast-supported cobbly-pebbly sandstone
Clast-supported cobbly sandstone (with occasional boulders)

Figure 14

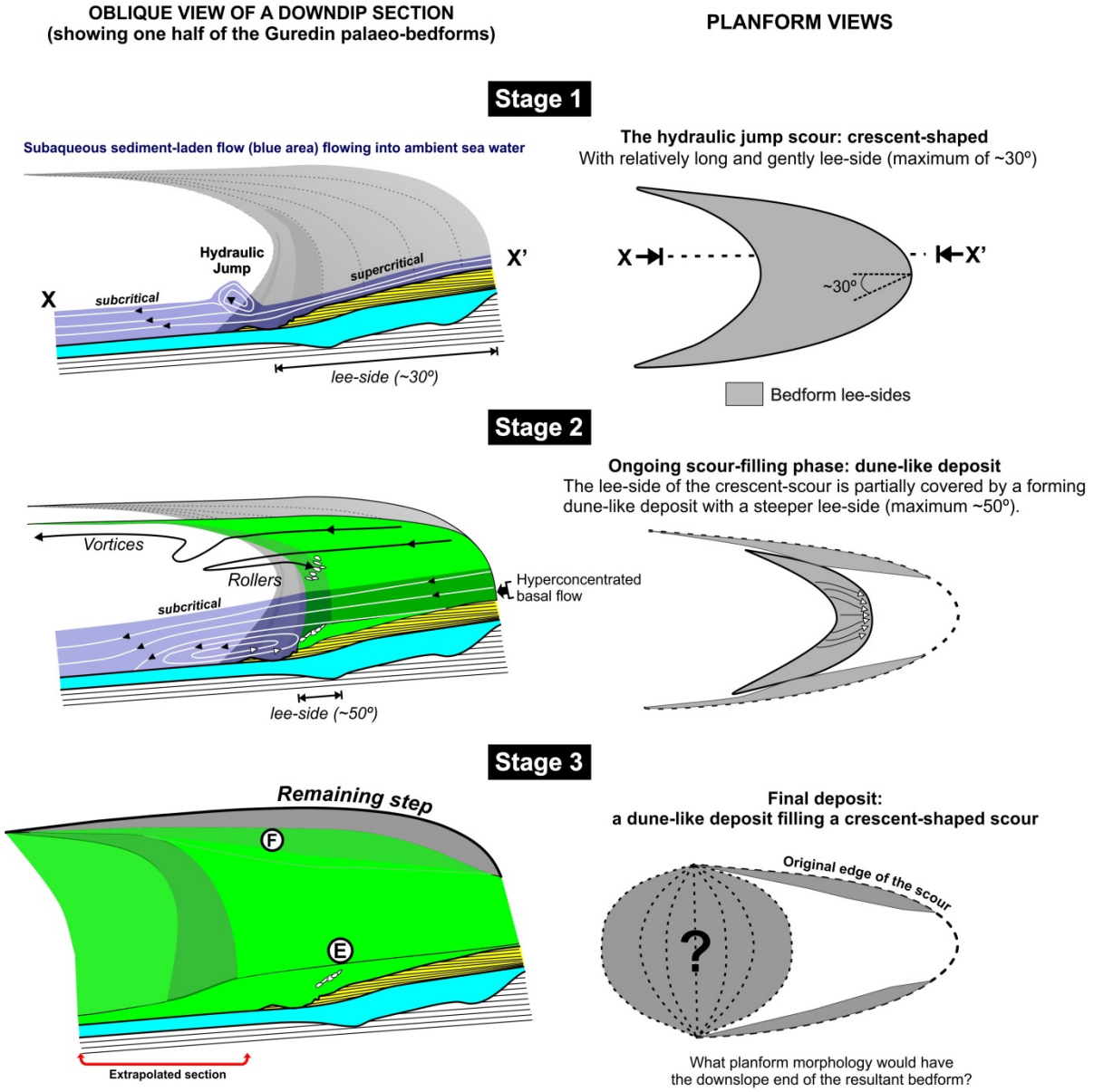
OBLIQUE VIEW OF A DOWNDIP SECTION
(showing one half of the Guredin palaeo-bedforms)
PLANFORM VIEWS
Stage 1
Subaqueous sediment-laden flow (blue area) flowing into ambient sea water
Hydraulic Jump
supercritical
subcritical
X
X'
lee-side (~30°)
The hydraulic jump scour: crescent-shaped
With relatively long and gently lee-side (maximum of ~30°)
~30°
Bedform lee-sides
Stage 2
Ongoing scour-filling phase: dune-like deposit
The lee-side of the crescent-scour is partially covered by a forming dune-like deposit with a steeper lee-side (maximum ~50°).
Vortices
Rollers
subcritical
Hyperconcentrated basal flow
lee-side (~50°)
Stage 3
Remaining step
F
E
Extrapolated section
Final deposit:
a dune-like deposit filling a crescent-shaped scour
Original edge of the scour
?
What planform morphology would have
the downslope end of the resultant bedform?

Figure 15

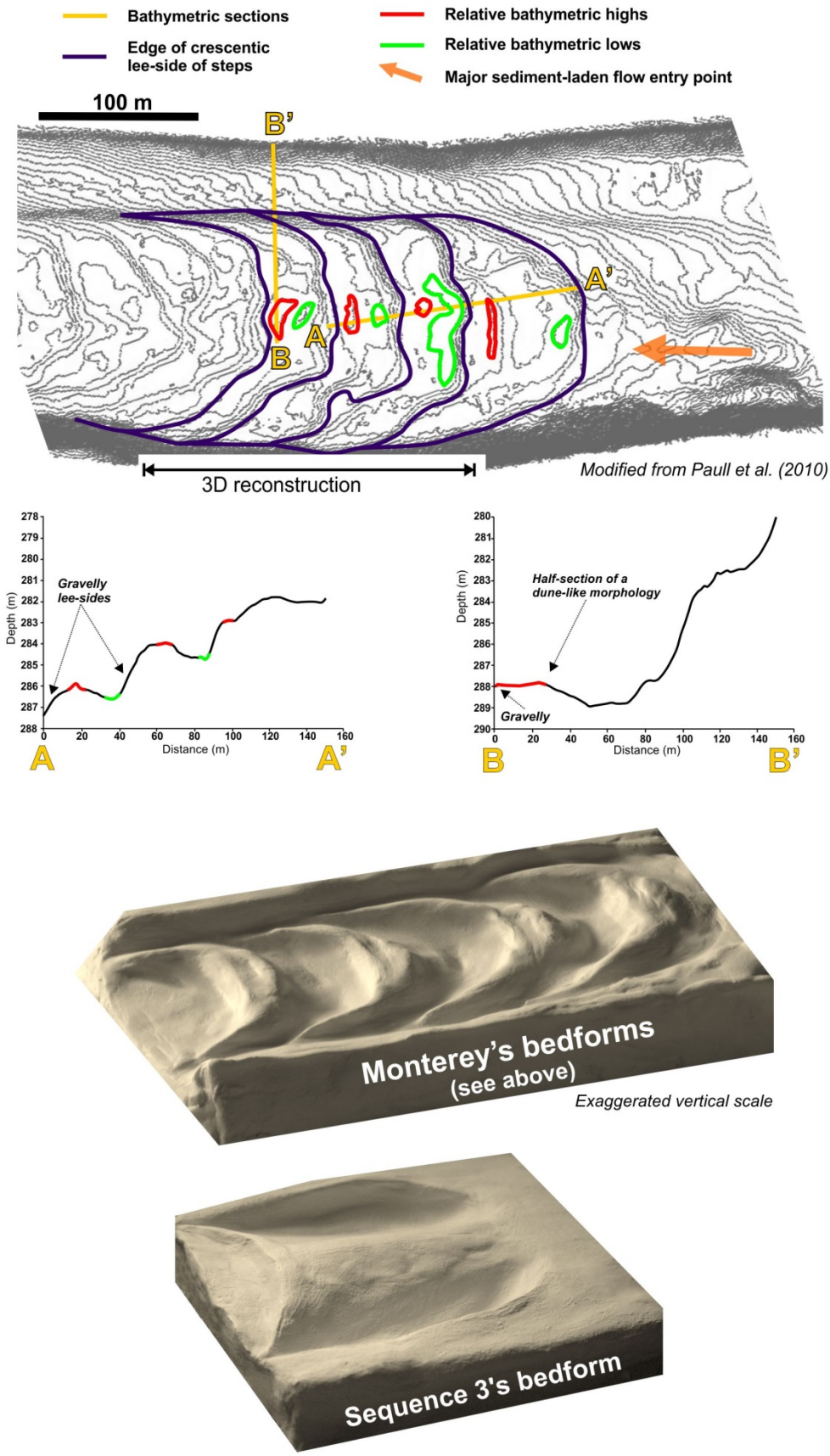
Bathymetric sections
Edge of crescentic lee-side of steps
Relative bathymetric highs
Relative bathymetric lows
Major sediment-laden flow entry point
100 m
B'
A'
A
B
3D reconstruction
Modified from Paull et al. (2010)
Gravelly lee-sides
Depth (m)
Distance (m)
A
A'
Half-section of a dune-like morphology
Gravelly
B
B'
Monterey's bedforms
(see above)
Exaggerated vertical scale
Sequence 3's bedform

Figure 16